Efficient removal of ultrafine particles from diesel exhaust by selected tree species: implications for roadside planting for improving the quality of urban air

Huixia Wang [1, 2], Barbara A Maher[2], Imad AM Ahmed[3] & Brian Davison[2]*

[1] School of Environmental and Municipal Engineering, Xi'an University of Architecture & Technology, Xi'an, 710055, Shaanxi Province, PRC

[2] Lancaster Environment Centre, University of Lancaster, Lancaster, LA1 4YQ, U.K.

[3] Department of Earth Sciences, University of Oxford, Oxford, OX1 3AN, U.K.

*Corresponding author: b.maher@lancaster.ac.uk

KEYWORDS: particulate matter (PM); human health; nanoparticles; deposition velocity; particle removal by leaf capture; magnetic particles; transition metals

ABSTRACT

Human exposure to airborne ultrafine (<<1 μm) particulate pollution may pose substantial hazard to human health, particularly in urban roadside environments where very large numbers of people are frequently exposed to vehicle-derived ultrafine particles (UFPs). For mitigation purposes, it is timely and important to quantify the deposition of traffic-derived UFPs onto leaves of selected plant species, with particularly efficient particle capture (high deposition velocity), and which can be installed kerbside, proximal to the emitting vehicular sources. Here, we quantify the size-resolved capture efficiency of UFPs from a diesel vehicle exhaust by nine temperate-zone plant species, in wind tunnel experiments. The results show that silver birch (79% UFP removal), yew (71%) and elder (70.5%) have very high capability for capture of airborne UFPs. Metal concentrations and metal enrichment ratios in leaf leachates were also highest for the post-exposure silver birch leaves; scanning electron microscopy shows UFPs concentrated along the hairs of these leaves. For all but two species, magnetic measurements demonstrate substantial increases in the concentration of magnetic particles deposited on the leaves after exposure to the exhaust particulates. Together, these new data show that leaf-deposition of UFPs is chiefly responsible for the substantial reductions in particle numbers measured downwind of the vegetation. It is critical to recognise that the deposition velocity of airborne particulate matter (PM) to leaves is species-specific; and often substantially higher (~10 to 50 times higher) than the 'standard' V_d values (e.g. 0.1 – 0.64 cm s^{-1} for $PM_{2.5}$) used in most modelling studies. The use of such low V_d values in models results in major under-estimation of PM removal by roadside vegetation, and thus misrepresents the efficacy of

selected vegetation species for substantial (>> 20%) removal of PM. Given the potential hazard to health posed by UFPs, and the removal efficiencies shown here (and by previous roadside measurements), roadside planting at PM 'hotspots' of selected species (maintained at or below head height) can contribute substantially and quickly to improvement in urban air quality, and reductions in human exposure. These findings can contribute to development and implementation of mitigation policies of traffic-derived PM on an international scale.

Introduction

1.1 Airborne particulate matter, and ultrafine particles

Airborne particulate matter (PM) is a health hazard on a global scale. Ultrafine particles (UFPs, aerodynamic diameter < 1000 nm), with a lifetime in the atmosphere ranging from a few seconds to several days, may pose particular risk to the health of the very large populations living, commuting and working in polluted urban environments, especially near major roadways[1]. UFPs have been shown to penetrate the respiratory system, enter the blood circulation, transfer to extra-pulmonary organs[2-3], and may also enter the brain directly via the olfactory bulb[4-5]. UFPs may be more toxic than microscale particles with the same chemical composition and at the same mass concentration owing to their very large surface area, increased chemical reactivity and ease of cell penetration[6-9].

Airborne UFPs can be derived both from anthropogenic and natural sources (e.g. biomass burning), but in many urban centres, motor vehicles are the primary emission sources of UFPs to the atmosphere, particularly in the morning and afternoon/evening rush hours[10-12]. Primary, vehicle-derived UFPs are produced directly from fuel combustion[13-14], engine wear[15] and from

45 frictional processes, especially brake wear[16-17]. Re-suspension of road dust provides multiple
46 opportunities for post-emission supply of airborne UFPs[18]. Primary, vehicle-derived UFPs are
47 often enriched in highly bioreactive transition metal species, especially Fe (both Fe^{2+} and Fe^{3+}),
48 Cu, Mn and Cr[12, 19], and other metals including Zn, Ni, V, and Pb[12, 20]. Secondary UFPs form in
49 the atmosphere through photochemical reactions involving gaseous precursors and post-
50 emission nucleation and condensation processes[10, 21].

51 Currently, policies for regulation of airborne PM are based on mass concentrations, of
52 PM_{10} and/or $PM_{2.5}$ (of aerodynamic diameter <10 μm or < 2.5 μm, respectively). The
53 contribution of UFPs to such mass-based metrics is minimal (< 10%), whereas they make up
54 ~80% or more of the PM number[14, 21-22].

55 Most of the PM emitted from vehicle exhausts lies within the $PM_{1.0}$ size range, with median
56 mass diameter between ~100 and 200 nm and a median number diameter of ~20 nm[23-24].
57 Emissions control strategies, based on engine design and after-treatment devices, have reduced
58 the average mass of particle emissions, but had limited success in reducing UFP numbers.
59 Indeed, some studies have reported increased UFP numbers[25] and increased UFP toxicity[26-27]
60 with the introduction of after-treatment devices. Hence, it is timely and important to identify
61 feasible and efficient technologies that can capture airborne UFPs, thus reducing human
62 exposure and damage to health.

63

64 *1.2 The effects of roadside vegetation on airborne PM: modelling and measurements.*

65 Roadside vegetation has the potential to decrease airborne PM concentrations, through PM
66 deposition on leaves, but also to increase PM concentrations, by impeding airflow and reducing
67 the dispersion of PM. As noted by recent reports[28], and reviews[29], many modelling-based
68 studies (using computational fluid dynamics, CFD, to simulate PM emission, dispersion and
69 deposition) have indicated rather small reductions, i.e. a few percent, in PM_{10} or $PM_{2.5}$
70 concentrations by deposition onto roadside vegetation[30-33]. If robust, such model-derived
71 outcomes indicate that roadside planting schemes are unlikely to produce any large reductions
72 ('> 20%') in PM_{10} or $PM_{2.5}$ concentrations. Indeed, AQEG[28] warns against 'campaigning zeal'
73 in 'popular publications' in communicating the likely improvements in air quality achievable
74 with roadside vegetation.
75 In a recent review[34] of some measurement-based (roadside, and wind tunnel) studies, the
76 reported removal efficiencies of PM concentrations by roadside vegetation vary enormously,
77 from enhancement of $PM_{2.5}$ (by up to 95%) to reductions (in, variably, PM, total suspended
78 particulates, UFPs, PM_1, $PM_{2.5}$, PM_{10}) of ~2 to 90%.
79 A fundamental factor appears to be key to both the parsimony of the model estimates and
80 diversity of the measured PM removal rates. That factor is the (mis)treatment of particle
81 deposition velocity (V_d) to leaf surfaces. Notwithstanding that particle deposition rates depend
82 on a range of factors, including particle diameter, PM concentration and wind speed, the critical
83 influence of *species-specific* leaf surface properties on controlling particle deposition rates,
84 capture, and agglomeration appears to have been under-recognised in measurement-based

85 studies, and substantially under-parameterised (i.e. typically by 5 to 50 times), in the majority
86 of CFD models[12, 35].

87 Leaf number, size, surface structures and the thickness, structure and composition of
88 epicuticular wax play critical roles in determining V_d and particle retention[36-40]. For example,
89 using magnetic particle loadings as a proxy for PM_{10}, Mitchell et al.[39] reported (magnetic) V_d
90 values varying for different plant species as a function of leaf micro-topography, especially
91 hairiness and rugosity. Lowest V_d values ranged from 0.5 to 0.9 cm s^{-1} for sweet chestnut, elder,
92 elm and willow; intermediate values from 1.3 to 1.9 cm s^{-1} for sycamore, horse chestnut, ash
93 and maple; higher V_d values, from 2.4 to 4.6 cm s^{-1}, for lime, beech and silver birch. Deposition
94 velocities of 10 cm s^{-1} have been reported for grassland[41] and Douglas fir for PM_{10}[42] while Freer-
95 Smith et al.[43] have reported V_d values exceeding 30 cm s^{-1} for maple, pine and cypress for $PM_{1.0}$.

96 In contrast, and critically, many modelling-based studies choose to use 'standard'
97 deposition velocity values as low as 0.64 cm s^{-1} or 0.1 cm s^{-1} for $PM_{2.5}$ [30, 44-45], or 0.2 cm s^{-1} for
98 PM_{10} [33]. Such values seem both low and indiscriminate, despite available data showing the
99 species-specific nature of this key term. It is therefore unsurprising (and indeed self-fulfilling)
100 that such modelling studies typically identify dominance of the aerodynamic (reduced
101 ventilation) over the depositional effects of roadside vegetation.

102 Based on the *measured* deposition velocities, then installation, close to the emitting vehicle
103 sources, of selected species with optimal V_d values, and controlled height and permeability, can
104 substantially reduce concentrations of traffic-derived PM (Fig. S1), whether at the roadside[46]
105 or in adjacent indoor environments.

For example, for a V_d of 4.6 cm s^{-1} (e.g. silver birch), and leaf surface area of 125 m^2/tree (canopy diameter 8m), 8 trees/100 m street length would remove 50% of the traffic-derived PM_{10} (Fig. S1). Such removal rates tally with published studies. In a street canyon setting, leaf capture of PM by young, roadside silver birch trees was associated with major reductions (60 – 80%) in adjacent indoor concentrations of $PM_{1.0}$, $PM_{2.5}$ and PM_{10}[12].

The orientation of roads in relation to predominant wind directions must also, of course, be taken into account, to ensure effective design of any newly-installed vegetation whether at the roadside, or within the roadway (e.g. as central lines, or lane separators).

Not only species selection but management is important since tall trees (> rooftop height) and high canopy density[47] can increase airborne PM mass concentrations, especially in street canyons, by obstructing airflow and reducing PM dispersion, effectively trapping the pollutants[33]. Additionally, some plant species can act as sources of biogenic volatile organic compounds (VOCs) to the urban atmosphere. For example, oxidation of isoprene, monotrepenes and sesquiterpenes can enhance secondary formation of $PM_{2.5}$ and of ground level ozone[48-50]. Albeit less hazardous than UFPs, the pollen of some species can trigger allergic rhinitis (hay fever).

For humid areas like Lancaster, the PM capture capability of birch leaves is renewed through PM wash-off by abundant rainfall[39, 51]. In drier areas, watering schemes might enable optimized PM removal by vegetation. The potential for contamination of the roadside soil[52] might require management, depending on the number of years of planned exposure time.

126 Depending on climate (especially humidity, rainfall), some species are likely to offer
127 permanent take-up of PM via particle entry through the leaf stomata, especially in the case of
128 waxy, evergreen leaves. Hence, combining tested, efficient, deciduous and evergreen species
129 might optimize PM removal through the entire year.

130 In terms of management, the selected roadside vegetation barrier, comprising selected,
131 high-deposition-velocity, PM-tolerant mixed evergreen and deciduous species, should be kept
132 well below roof height[35], and pruned to prevent development of a dense canopy crown, in order
133 to facilitate atmospheric dispersion of PM. Selected species of trees, managed as hedges
134 ('tredges'©), may thus provide the best option for immediate improvement of air quality,
135 especially in PM 'hotspots', wherever the most, and the most vulnerable people (e.g. young
136 children) receive the greatest PM exposure.

137 *1.3 Vegetation impacts on UFPs*

138 Despite their abundance in the urban atmosphere and their potential toxicity, UFP removal
139 by plants has so far received relatively little attention. Field measurements to quantify the
140 influence of urban plants on UFPs and particle number concentrations (PNCs) are few. In
141 Raleigh, Carolina, Baldauf et al.[53] found PNCs reductions of 15 – 50% at distances up to 10s
142 of metres behind a (discontinuous) noise barrier; combined noise and vegetation barriers
143 consistently reduced the PNCs more efficiently than noise barriers alone.

144 For a major road in Guildford, UK, Al-Dabbous and Kumar[54] reported ~37% reduction
145 in PNCs by a coniferous vegetation barrier, during intervals with cross-road wind directions.
146 Lin et al.[55] reported 38 to 64% reduction in UFPs (14 to 102 nm) concentrations behind a

147 deciduous roadside vegetation barrier when in leaf, but no reduction in winter without
148 foliage.

149 Fewer studies have examined the effects of different types of vegetation on reducing UFP
150 numbers. Using pine and juniper branches in a wind tunnel, Lin and Khlystov[56] found UFP
151 removal efficiency to be directly proportional to the vegetation packing density, and inversely
152 proportional to particle size and wind speed. Freer-Smith et al.[43] found that V_d values were
153 dependent on plant species, particle size and ambient PM concentrations. For some coniferous
154 species, they reported V_d values for UFPs as high as 25 to 36 cm s^{-1} at a busy road, and 12 to
155 30 cm s^{-1} at a parkland site. Hwang et al.[57] studied five different vegetation types in a deposition
156 chamber. They reported higher V_d for UFPs for needle leaf compared with broadleaf trees; the
157 leaf surface roughness also influenced the deposition efficiency.

158 In summary, a limited number of studies has examined the removal efficiency of traffic-
159 produced UFPs by different plant species. Given limited space in urban areas, it is important
160 that the most effective plant species for UFP removal should be selected for urban greening.
161 Here, we examine, in a wind tunnel, the size-resolved removal of UFPs by nine plant species:
162 silver birch (*Betula pendula*), yew (*Taxus baccata*), nettle (*Urtica fissa*), beech (*Fagus*
163 *sylvatica*), cherry (*Prunus avium*), elder (*Sambucus nigra*), maple (*Acer campestre*), hawthorn
164 (*Crataegus monogyna*) and ash (*Fraxinus excelsior*). Our new data indicate that selected plant
165 species can remove by surface deposition substantial amounts (> 50%) of ultrafine exhaust-
166 derived PM, and of the heavy metals contained within the high particle number concentrations
167 of this PM fraction. Fast, non-destructive magnetic measurements provide an effective

indicator of leaf particle deposition. Scanning electron microscopy can identify the major leaf micro-sites associated with greatest particle accumulation. Hence, roadside planting of carefully-selected and managed plant species can effectively mitigate exposure of road users and adjacent residents (especially vulnerable groups like school children) to UFP pollution near major roads. Careful testing and selection of the most efficient species can readily improve air quality.

2. Experimental methods

2.1 Plant Species

UFP removal efficiency was measured in a rectangular wind tunnel (200 cm long, 75 cm wide, 75 cm high, Fig. S2). Nine plant species with different leaf surface characteristics and particle deposition velocities were selected based on our previous study[39], including silver birch, yew, nettle, beech, cherry, elder, maple, hawthorn and ash. These species are widespread in temperate regions, have different leaf retention behavior (i.e., deciduous vs evergreen species) and different leaf morphologies (i.e., broad leaves vs needles) and micro-topographies, which are expected to have an influence on UFP deposition and accumulation (Table S1, Supporting Information).

To obtain 'clean' leaves, plant species were collected after rainfall from Lancaster University campus (maple, ash, hawthorn, beech, cherry, elder) and Williamson Park, Lancaster (yew, silver birch, nettle), as far as possible from roads. Branches (~60 cm in length) of each species, freshly cut on the day of the measurements, were supported vertically

and uniformly as a vegetation block (i.e. with very similar leaf area index, LAI, values, Table S1) to ensure that most of the air stream passes through them (Fig. S2, Supporting Information). Particles were emitted from the exhaust of an idling diesel engine (2.1 litre, with catalytic converter; BS EN590 Standard diesel fuel), and injected via smooth plastic tubing into the wind tunnel. A fan positioned at the centre of the front sidewall was used to produce steady airflow, of 1.0 m s^{-1} (typical for the Lancaster area in summer[58], and to mix the exhaust stream with the airflow.

2.2 Particle number concentrations and size distributions

A GRIMM model 5.400 scanning mobility particle sizer (SMPS), comprising a long differential mobility analyser (DMA, model 5.5-900), was used to measure particles in 44 size categories, between 9.8 and 874.8 nm, to obtain the size distribution and count PNCs over consecutive 7 min intervals. Particle sampling was carried out via plastic tubing (~60 cm) connected first to a sampling port located upwind (~20 cm) and then downwind (~20 cm) of the vegetation, to sample continuous PNCs and particle size distributions. PNCs and size distribution measurements were first made in the absence of any vegetation for four separate 7 min. intervals. Measurements were then made first, upwind and then, downwind of the different vegetation species, over successive sampling durations; 5 × 7 mins for each plant species. For each of the plant species, the collection efficiency was measured at a wind speed of 1.0 m s^{-1}, typical in summer in the study area (Lancaster, U.K.).

209 At the end of the experiment, ~5% of the total leaves from each vegetation block was
210 weighed (Oertling KC22 microbalance) then scanned, and leaf area measured through counting
211 image pixels. Total foliage area was determined by the mass proportion of the scanned leaf
212 weight to total weight and leaf area; the total leaf area was divided by the crown area to
213 determine the LAI, to ensure comparability between the species removal efficiencies (the LAI
214 values varied very little, from 7.2 to 8.8, Table S1).
215 Leaf samples of each species were collected before exposure to the diesel exhaust (here
216 labelled as 0 minutes) and then after successive exposure intervals (i.e. after 2, 5, 10, 20, 30,
217 and 35 minutes), using gloves to avoid contamination. The leaves were stored (upper surface
218 to upper surface) in ziplock bags, at 4 °C, prior to scanning (5-6 leaves per individual species
219 sample), and then packed into 10 cm^3 plastic pots for magnetic measurements (at the Centre
220 for Environmental Magnetism and Palaeomagnetism, Lancaster University).
221
222 *2.3 Magnetic measurements*
223 Measurements were made of anhysteretic remanent magnetization (ARM) and the
224 saturation remanence (SIRM) of the leaves pre- and post-exposure (see Supporting
225 Information). ARM is sensitive to the presence of ferrimagnetic particles with a mean particle
226 size of ~25 nm[59]. The SIRM indicates the total concentration of magnetic particles on the pre-
227 and post-exposure leaves. ARM was induced using a Molspin A. F. demagnetiser, with ARM
228 attachment, generating a dc biasing field (0.08 mT) in the presence of an alternating field (100
229 milliTesla (mT) peak field). The ARM was measured using a spinner magnetometer (JR-6A,

AGICO). The susceptibility of ARM (χ_{ARM}) was calculated by normalizing the ARM by the dc biasing field.

Room temperature remanent magnetization (IRM) was then incrementally acquired (in dc fields of 100 and 300 mT) using a Molspin pulse magnetizer. Calibration of the magnetometer was performed, on a regular basis, using a cross-calibrated rock sample (56.05×10^{-8} Am^2). All samples were measured in triplicate; the average value of each magnetic parameter was normalised for the leaf surface area (in m^2).

2.4 Metals analysis

The leaf-deposited PM was also evaluated by an acid wash procedure and analysis of metal concentrations using inductively coupled plasma-mass spectrometry (ICP-MS). Two leaves from each species, pre- and post-exposure, were washed thoroughly using purified 2% HNO_3 (the background metals concentration in 2% HNO_3 shown in Fig. S3) into acid-cleaned centrifuge tubes. The resultant, replicate leachates were then analysed for Mn, Fe, Co, Ni, Cu, Zn, Ti, V, Cr, As, Zr, Mo, Se, Cd, Sn, Sb, Pt and Pb using a Perkin Elmer quadrupole NexION 350D ICP-MS instrument. The metal concentrations reported here represent the average concentrations. The elements Se, Cd, Sn, Sb, Pt and Pb were measured under non-pressurised conditions (standard mode) whereas the remaining elements were measured in a collision cell with kinetic energy discrimination (collision mode) using helium gas. Metal compositions in the stock acid wash solution were well below 25 ng L^{-1}, except for

Ti (< 65 ng L^{-1}) and Zn (< 201 ng L^{-1}), most likely a contribution from tubing used during the ICP-MS analysis.

2.5 Electron Microscopy

To identify UFP capture sites, leaves of the most effective species (silver birch) were examined using scanning electron microscopy (SEM) and energy dispersive spectroscopy (EDAX). Three leaf discs (10 mm diameter) of the pre- and post-exposure silver birch leaves were cut with a clean ceramic blade and coated with a thin layer (< 5 nm) of gold using an ion sputter. Each leaf disc was degassed (for 3 h at 0.7 bar), mounted on an aluminium stub over double-sided sticky tape and their microstructure examined with an SEM (FEI Quanta 650, FEI, Hillsboro, Oregon, USA) operating at an accelerating voltage of 10 or 20 kV. Elemental mapping was performed with an Oxford energy-dispersive X-ray spectrometer (EDAX). To reduce detection levels below the typical limit (~1000 ppm by weight), spectra were collected after acquisition times of up to 5 min. At least 5 spots from each leaf (before and after exposure) were analysed by EDAX.

2.6 *Statistical Analysis.*

Removal efficiencies were calculated using the following equation:

$$R_{eff(i)}(\%) = \frac{PNC_{upwind(i)} - PNC_{downwind(i)}}{PNC_{upwind(i)}} \times 100 \quad (1)$$

where R_{eff} (%) is the removal efficiency, PNC_{upwind} is the particle number concentration upwind in the wind tunnel experiment (#/cm^3), $PNC_{downwind}$ is the PNC downwind (#/cm^3),

and i is the different particle size bins (i.e., 9.8-874.8 nm, 9.8-30 nm, 30-100 nm, 100-300 nm and 300-874.8 nm).

The Kolmogorov-Smirnov and Levene tests were used to verify the assumption of normality and the homogeneity of variances for the magnetic data (ARM, IRM_{100}, IRM_{300} and SIRM) and metal concentrations. One way analysis of variances (ANOVA) was carried out to investigate the effects of the plant species, and time intervals on the magnetic data. The significance of differences among the plant species were checked with Tukey's test (p = 0.05). The differences in metal concentrations among plant species were also tested by ANOVA and Tukey's test. Differences in metal concentrations between pre- and post-exposure leaves were tested using student's t test for each species. The data were analysed with SPSS software (ver. 20.0, IBM Corp, Armonk, NY).

3. Results and discussion

3.1 *UFP removal efficiency of different plant species*

The measured mean PNC for the diesel exhaust (in the absence of vegetation) was ~$25\times10^5/cm^3$ (Fig. 1). There is no obvious increase in PNC upwind of the tested vegetation species compared with the no-vegetation case (Fig. S3, Supporting Information); occasionally, the upwind PNCs are slightly lower, perhaps indicating some upward deflection of UFPs away from the central CPC measurement point.

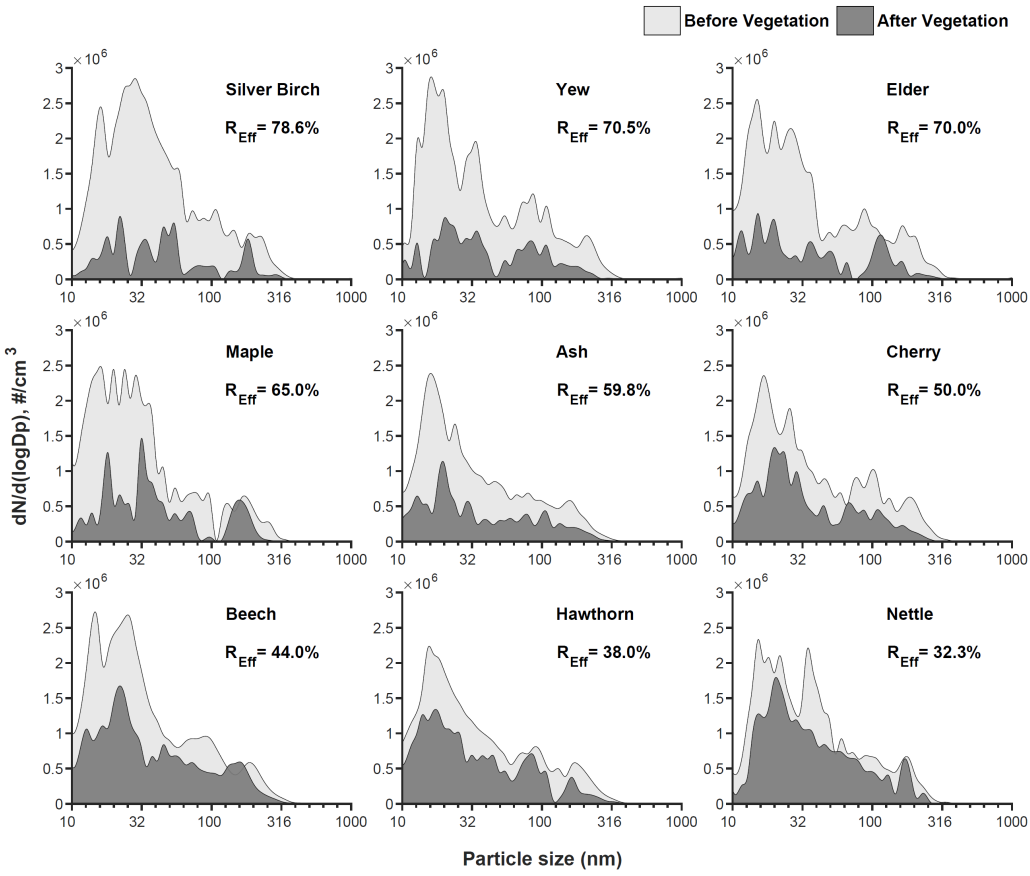

Fig. 1. Mean particle number distribution pre- and post-exposure (35 mins) of each vegetation species to the diesel exhaust ('Before Vegetation' = upwind of vegetation block; 'After Vegetation' = downwind of vegetation block). R_{Eff} (%) indicate the removal efficiency of UFPs by each species.

The average number size distributions of the UFPs, both in the absence of, and upwind and downwind from the vegetation displayed two major peaks, at 16 and 26 nm (nucleation mode), and a subsidiary peak of accumulation mode (soot) particles at ~100 nm (Figs. 1 and S3). This distribution showed little change upwind and downwind for most of the plant species investigated, indicating the permeability of each tested vegetation block to the air stream. In marked contrast, measurements of $PM_{2.5}$ (by TSI, USA, SidePak AM520) upwind and

306 downwind of a dense conifer species (juniper) identifies 'blocking' of air flow and resultant
307 upwind enhancement of PNCs (Fig. S4). Some species induced slight increases in downwind
308 mean particle size (see below).

309 Compared to the no-vegetation measurement, significant PNC reduction was measured
310 downwind of most species tested, with much of the reduction occurring for the smaller particle
311 sizes. Different plant species resulted in different removal efficiencies, reducing PNCs by up
312 to ~79%. Silver birch is the most efficient species in removing UFPs, followed by yew>elder
313 > maple > ash> cherry > beech > hawthorn > nettle (Fig. 1).

314 When the diesel exhaust had passed through the vegetation, the geomean diameter showed
315 small but measurable increases, except in the case of hawthorn, elder and cherry (Table S3,
316 Supporting Information). Silver birch and yew showed the largest mean increase in particle
317 size, from 20.8 to 27.2 nm, and 19.3 to 29.6 nm, respectively, followed by maple (from 18.5 to
318 23.8 nm).

319 Dividing the PNC data into four size bins, 9.8–30 nm ($N_{9.8-30}$; nucleation mode), 30–100
320 nm (N_{30-100}; Aitken mode), 100–300 nm ($N_{100-300}$; accumulation mode) and 300–874.8 nm
321 ($N_{9.8-30}$; coarse mode), the plants displayed differences in their removal of different particle
322 size ranges (Fig. 2). For the nucleation mode (9.8–30 nm), silver birch removed the greatest
323 particle numbers, followed by yew > elder > maple > cherry > ash > hawthorn > nettle. The
324 nine different plant species followed this same order of removal efficiency for the PNCs in
325 the accumulation and coarse modes.

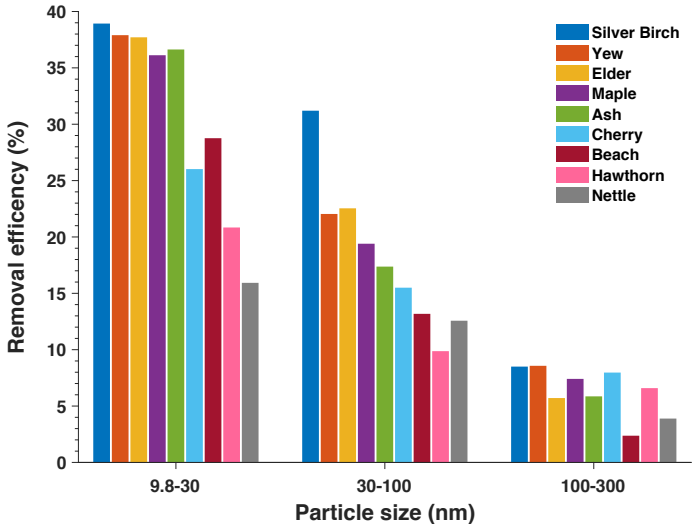

Fig. 2. The UFP removal efficiency of different plant species for different particle size bins.

3.2 Leaf magnetic values, magnetic mineralogy and grain sizes.

The pre- and post-exposure leaves display differences in ARM, IRM_{100}, IRM_{300} and IRM_{1000} (Fig. 3 A and B). The nettle and hawthorn displayed the highest pre-exposure magnetic content. For all but the hawthorn, the magnetic particle loadings on the leaves increased after their exposure to the diesel exhaust (Figs. 3 and S4 and 5; Fig. S3, Supporting Information). The ARM, IRM_{100}, IRM_{300} and SIRM of pre-exposure leaves ranged from ~5.0 to 22 $\times 10^{-8}$A, 0.7 to 3 $\times 10^{-6}$A, 1 to 4 $\times 10^{-6}$A, and 1 to 4 $\times 10^{-6}$A, respectively. The ARM, IRM_{100}, IRM_{300} and SIRM values of the exposed leaves ranged from ~13 to 35$\times 10^{-8}$ A, 1 to 4.5 $\times 10^{-6}$A, 2 to 6 $\times 10^{-6}$A, and 2 to 6$\times 10^{-6}$A, respectively.

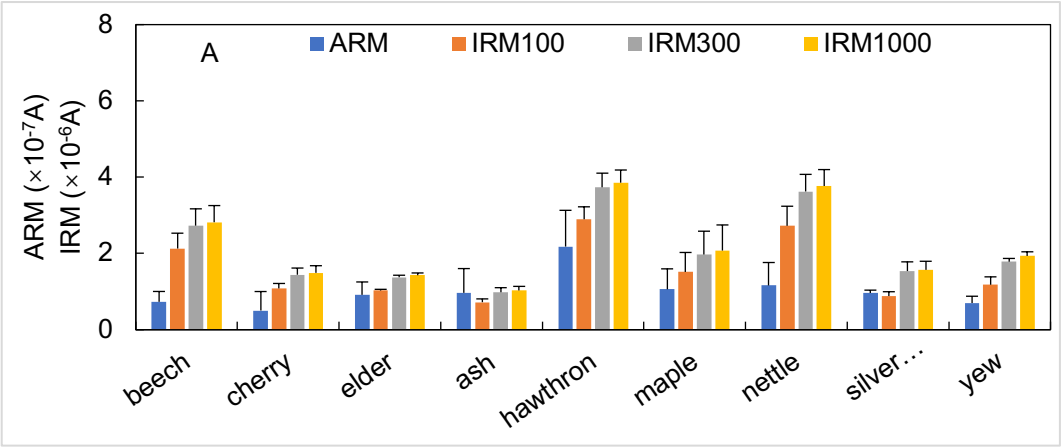

339

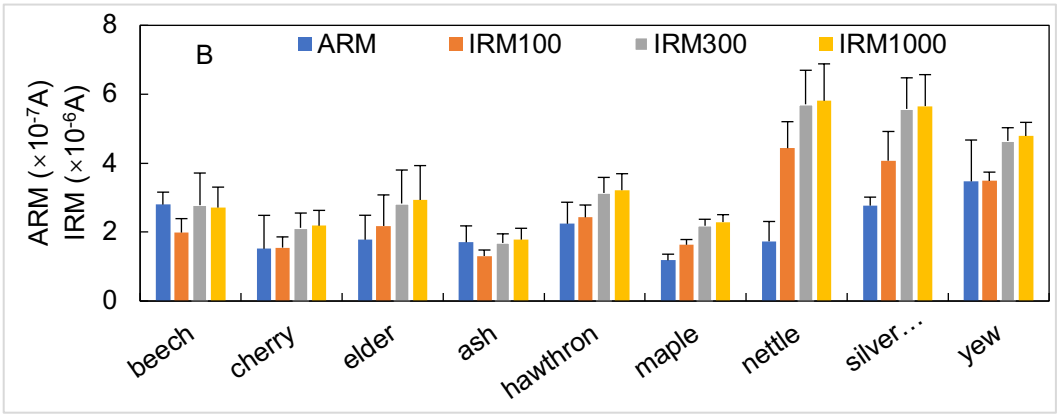

340

341 Figure 3. (A) Pre- and (B) post-exposure leaves display differences in magnetic particle

342 loadings, as measured by ARM, IRM_{100}, IRM_{300} and IRM_{1000}

343

344 For each species, the leaf magnetic particle loadings, as measured by ARM, IRM_{100}, IRM_{300}

345 and IRM_{1000}, vary through the successive periods of exhaust exposure. The silver birch leaves

346 showed both the highest rate and most continuous accumulation of magnetic particles through

347 the whole exposure period, followed by yew and elder, and then maple and nettle (Fig. S5,

348 Supporting Information). Hawthorn showed little magnetic difference between pre-experiment

349 and post-exposure leaves (Fig. S5B). Elder, maple, ash, cherry, beech and nettle all appear to

350 reach a dynamic equilibrium (i.e. particle deposition balanced by particle re-suspension) in

351 magnetic particle loadings within the timespan of the experimental exposure.

All leaves acquired most magnetic remanence at low applied fields; ~ 70% by 100 mT, and 95% by 300 mT (Table S2, Supporting Information). This indicates the presence of magnetically "soft" material (i.e., easily magnetized and demagnetized), such as magnetite (Fe_3O_4). Between 8% and 30% of the SIRM was acquired at higher applied fields (100 to 300 mT), indicating the presence of some maghemite and/or some nanoparticulate haematite[60]. The acquisition of some additional remanence (mostly ~1 to 2%, max 8%) at highest dc fields (> 300 mT) shows that magnetically 'hard' haematite also contributes to the leaf magnetic mineralogy. Given that haematite is much more weakly magnetic than magnetite, then up to ~40 times more haematite than magnetite may have deposited on the leaves during exposure to the diesel exhaust stream.

The different plant species also showed different leaf χ_{ARM}/SIRM values after exposure to the exhaust. Silver birch leaves had the highest χ_{ARM}/SIRM values, ranging from 62 to 138 $\times 10^{-5} A^{-1}$, with successive increases with exposure time. Because ARM is particularly sensitive to the presence of ultrafine magnetite particles, around 30 nm in size[59], χ_{ARM}/IRM_{300} values can be used as a rough estimate of magnetite grain size.

The magnetic particles present on the pre-exposure silver birch leaves were in the size range of ≤ 100 nm (Fig. S6, Supporting Information). After 20 minutes' exposure to the diesel exhaust, the magnetic grain size of the particles deposited on the silver birch leaves decreased to ~ 20 nm in size. When the exposure time increased from 20 to 35 mins, the magnetic particle size increased to ~70 nm. In contrast, the size of the magnetic particles on nettle leaves was in the range of ~200 – 600 nm (Fig. S6, Supporting Information).

373

374 3.3 Metal concentrations of leaf-deposited PM

375 The concentrations of Mn, Fe, Cu and Zn on the post-exposure leaves were much higher
376 than the other metals analyzed (Fig. 4). The metal contributions, post-exposure, are as
377 follows: Mn > Zn > Fe > Cu > Ni > Ti > Cr > Pb > As > Se >Cd > V > Co > Zr > Mo > Pt.
378 The very high Mn concentrations probably arise from the use of the diesel fuel additive,
379 methylcyclopentadienyl manganese tricarbonyl (MMT) and/or from engine, especially
380 cylinder, wear. The latter source, together with lubricating oil, is also likely to contribute the
381 observed concentrations of Zn, Fe, Cu, and Cr[13]. The post-exposure metal concentrations
382 from the leaf-deposited PM differed significantly between plant species
383 (Fig. 4 and Table S4, Supporting Information). The highest metal concentrations were found
384 in the leaf leachates from the silver birch, followed by yew and maple.

385

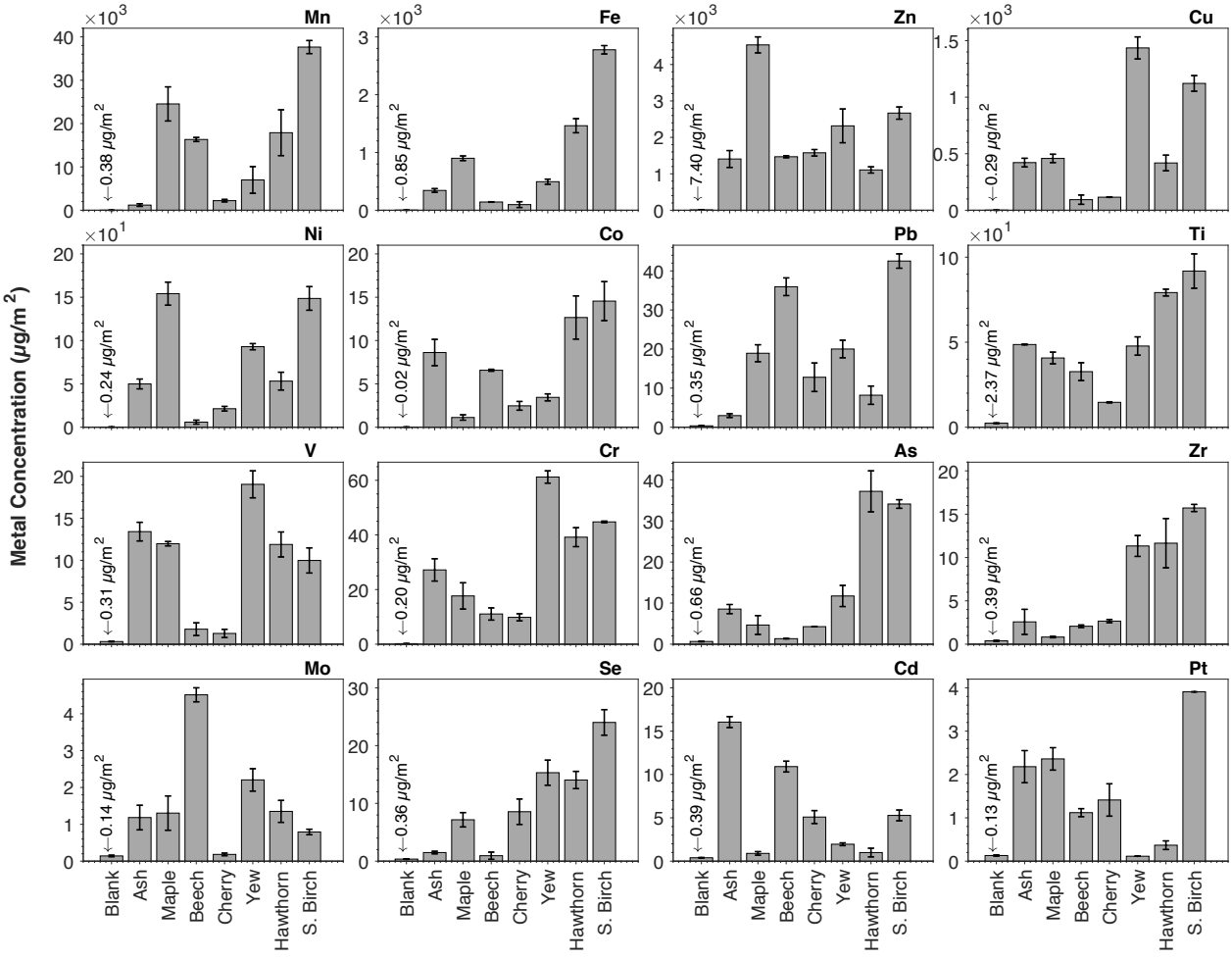

386

387 Fig. 4 Metal concentrations of leaf leachates post-exposure (i.e. metal concentrations$_{post\text{-}exposure}$

388 – metal concentrations$_{pre\text{-}exposure}$). ICP-MS data expressed as µg metal per m^2 of leaf surface area.

389

390 3.4 SEM-EDX

391 Scanning electron micrographs (Figs. 5 and 6) show the typical rough, hairy morphology

392 of the adaxial leaf surfaces of the most efficient species, silver birch, which is hypostomatic

393

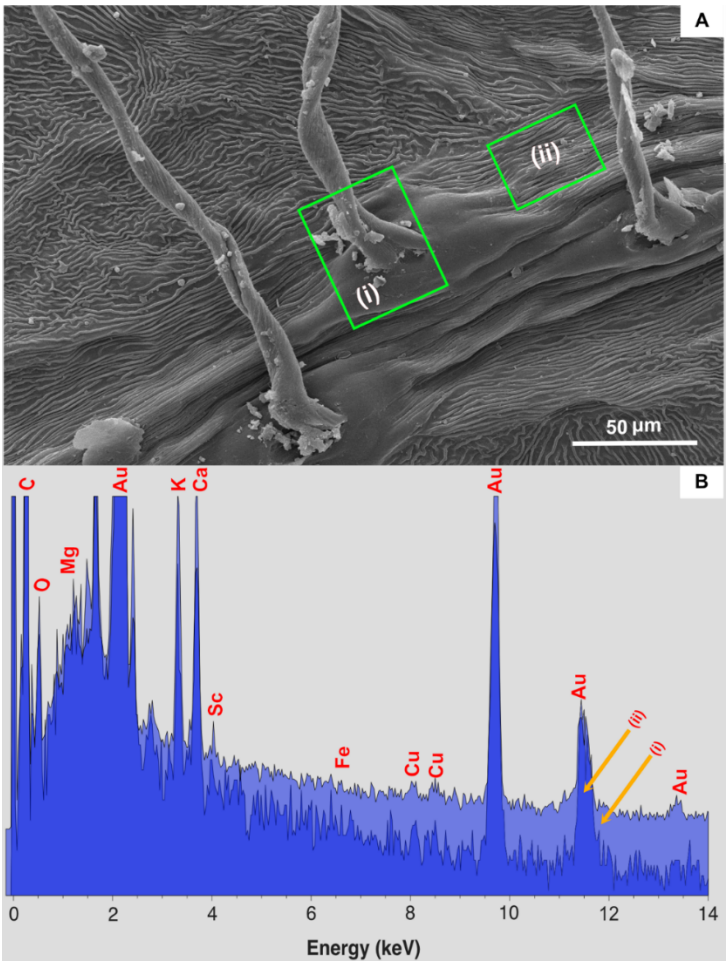

394

395

396 Fig. 5 (A) Scanning electron micrograph of the adaxial surface of the pre-exposure silver birch

397 leaf, and (B) EDAX spectra for the leaf-deposited PM in sub-areas (i) and (ii) of image (A).

398 (Note that the sample was gold-coated).

399

400 i.e., stomata occur only on the underside of the leaves. SEM-EDAX analysis of the silver birch

401 leaf surfaces shows very low content of transition metal-bearing PM on the pre-exposure leaves

402

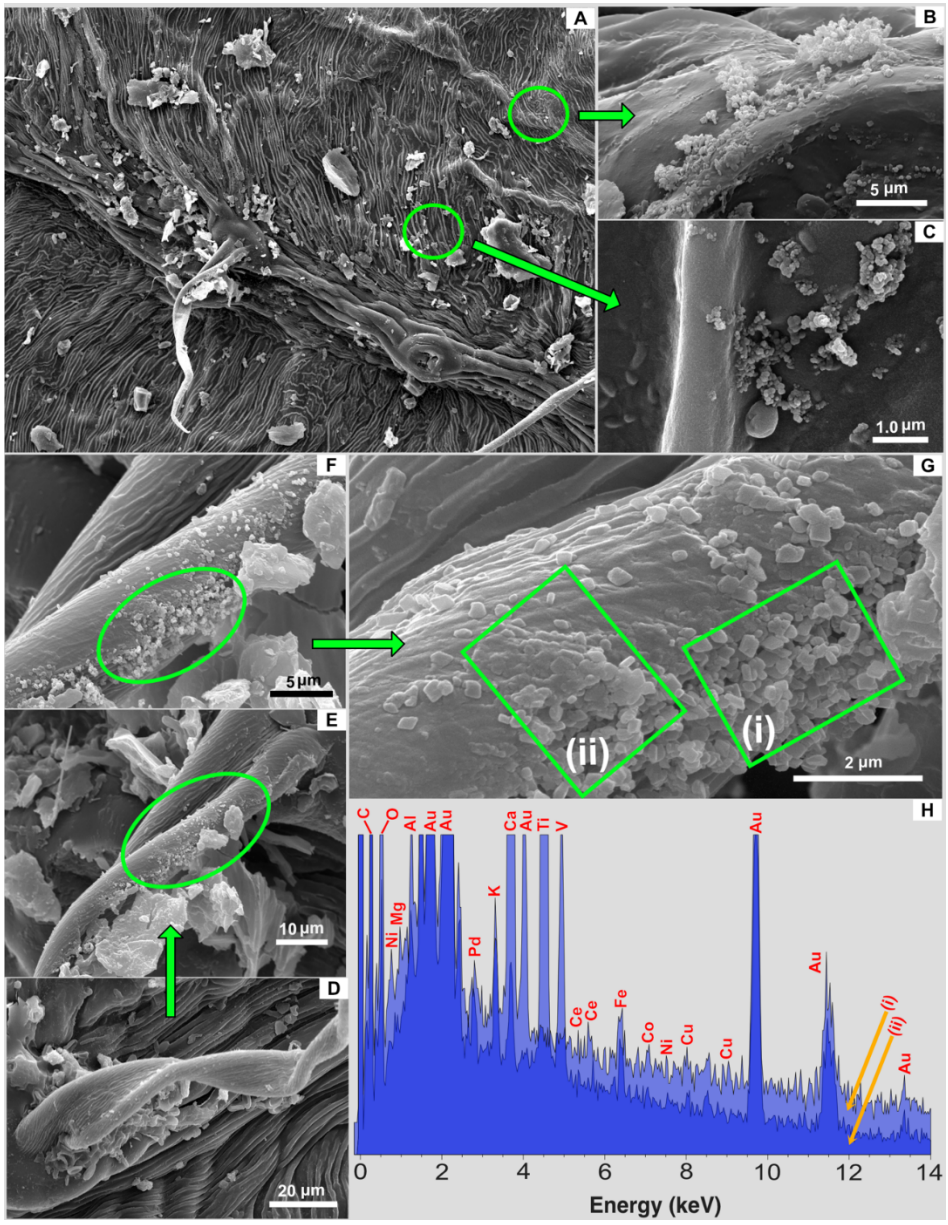

403

404 Fig. 6 (A) – (G): Scanning electron micrographs of the post-exposure silver birch leaves, and

405 (H) EDAX spectra of the deposited particles shown in areas (i) and (ii) in micrograph (G).

406

407 (Fig. 5). In contrast, post-exposure, the silver birch surface displays an abundance of particles

408 within the $PM_{2.5}$ range (Fig. 6), displaying a range of particle sizes and morphologies, including

409 aggregated rounded chains of particles (Fig. 5C and Fig. S7), and discrete geometric particles

410 (Fig. 6G). The post-exposure accumulation of UFPs within the micro-indentations of the rough

411 leaf surface, and along and around the leaf hairs is noteworthy. These locations appear to be
412 'hot spots' for capturing UFPs; and may also act as gateways for UFP access to the leaf interior
413 structure.

414 Prior to exposure, the major PM elemental contributions comprise C, O, Mg, K, and Ca
415 (Fig. 5B). In contrast, the post-exposure birch leaves display higher concentrations of UFPs
416 containing a much broader elemental range; specifically, the presence of Ni, Fe, Ti, V, Ce,
417 Al, Pd, Cu and Co (Fig. 6H).

418

419 **4. Discussion**

420 These wind-tunnel experiments show that some plant species (silver birch, yew, elder,
421 maple and ash) display UFP removal efficiencies as high as ~60 to 80%, demonstrating that
422 selected plant species can act as effective UFP 'sinks' in the urban environment. Similar
423 magnitudes of PM removal have been reported in real-world contexts for silver birch (for $PM_{1,}$
424 Maher et al.[12]), and mixed woodland in Birmingham, U.K. (for PM estimated at 0.7 μm, Fowler
425 et al.[52]).

426 Silver birch displayed both peak UFP removal values (~80%) and peak removal of
427 particles < 30 nm. It continued to accumulate the finest magnetic particles (< ~20 nm) for 20
428 mins. of exposure, and then accumulated slightly larger and/or agglomerated PM (~70 nm)
429 through to the end of the experiment. It is thus the most efficient of our sampled species in
430 removing diesel exhaust UFPs; followed by yew and elder. Some of the sampled species (e.g.

ash, cherry) display magnetic evidence of both particle deposition and re-suspension through the time sequence of exposure.

Although nettle and hawthorn appear to be the least efficient plant species, their pre-exposure magnetic particle loading was higher than the other sampled species. This suggests they may have been 'pre-loaded' with airborne PM, and effectively at or close to a dynamic equilibrium between the rates of particle deposition and loss by re-suspension. In the real world, leaves can continue to accumulate particles (rather than attain equilibrium with ambient PM concentrations) through rainfall wash-off[39] and entry of PM into the leaf structure via stomata and/or wax cuticle overgrowth[61].

Leaf surface characteristics and size appear critical regarding PM deposition. Particles are more readily deposited on smaller leaves, with shorter petioles, surface roughness, especially in the form of leaf trichomes, and/or mucilage[12, 36, 38-39, 62-64]. Phoretic effects, in response to gradients in turbulence[65]), chemical and/or electric potential[66], may enhance UFP deposition along leaf hairs.

Here, we also found that when the diesel exhaust passed through some of the sampled species, the geomean diameter increased downwind of the vegetation, showing that these plants (silver birch, yew, maple) removed more of the smallest UFPs, possibly of greatest potential hazard to human health.

For our most efficient species, silver birch, many of the UFPs deposited on the post-exposure leaves were rich in transition metals, including Mn, Ni, Fe, Al, Cr, V, Ti and Cu, together with the anti-knock and catalytic converter metals, Ce and Pd. Most of the magnetic

452 remanence-capable particles deposited on the post-exposure silver birch leaves were < 100 nm.
453 Nanoparticles of this size can penetrate the body very efficiently[2], even bypassing the blood-
454 brain barrier via the olfactory bulb[4-5]. Similarly, Maher et al.[5, 12] found that many particles
455 deposited on the leaves of silver birches installed at a busy roadside (Lancaster, U.K.) were <
456 200 nm, exhibited spherical or semi-spherical morphologies, and were Fe-rich. Such Fe-rich
457 particles, abundant and typical of condensation droplets released from high-temperature
458 combustion and frictional (brakewear) processes, are likely to contribute much of the measured
459 magnetic remanence of the plant leaves. Particles rich in transition metals might cause
460 oxidative stress by direct generation of reactive oxygen species not only in lung and
461 cardiovascular cells but also in the brain[5]. Oxidative brain damage is a characteristic of most
462 types of neurodegenerative disease, including Alzheimer's and Parkinson's disease.

463 All of the data reported here are consistent with the efficient interception and capture of
464 vehicle-derived UFPs by plant leaves, rather than airflow impedance or perturbation, or
465 physical screening effects and "fumigation" of the upwind zone. (In marked contrast, similar
466 experiments on juniper indicate 'blocking' of airflow, and resultant enhancement of upwind
467 PNCs).

468 Given the health impacts of exposure to traffic-derived PM, it is essential to understand,
469 and optimise, the mitigation potential of roadside vegetation, in order to guide policy
470 appropriately. In the UK, for instance, even reducing the annual average concentration of $PM_{2.5}$
471 by only 1 $\mu g/m^3$ would result in a saving of ~3.6 million life years, equivalent to an increase in
472 life expectancy of 20 days in people born in 2008[67]. It is thus timely to improve and update the

473 available data and information regarding PM removal rates by leaf deposition, in order to
474 optimise selection and design of new roadside planting.

475 Under-estimation by most CFD modelling studies of the potential for substantial PM
476 removal by designed vegetation has negative impacts on policy and potential mitigation.
477 Adoption of realistic, species-specific particle deposition velocities (i.e. up to ~50 times higher
478 than the values of 0.1, 0.2 and 0.64 cm s^{-1} commonly employed for $PM_{2.5}$) and an appropriate,
479 microscale approach, at road user-relevant heights[35], are both essential.

480 In summary, these data indicate that selected plant species can remove by surface
481 deposition substantial amounts (> 50%) of ultrafine exhaust-derived PM, and of the heavy
482 metals contained within the high particle number concentrations of this PM fraction. Fast, non-
483 destructive magnetic measurements provide an effective indicator of leaf particle deposition.
484 Scanning electron microscopy can identify the major micro-sites associated with greatest
485 particle accumulation. Hence, roadside planting of carefully-selected and managed plant
486 species can effectively mitigate exposure of road users and adjacent residents (especially
487 vulnerable groups like school children) to UFP pollution near major roads. Careful testing and
488 selection of the most efficient species can readily improve air quality.

489 **Acknowledgements**

490 We are grateful for financial support from Natural Science Basic Research Plan in Shaanxi
491 Province of China (2017JQ4014) and the Research Program of Ministry of Housing and Urban-
492 Rural Development of the People's Republic of China (2018-K2-006). We also are grateful to

493 Andy Baker, Engineering Department, Lancaster University for assistance with the wind tunnel
494 and the diesel vehicle.

495

496 **Supporting Information Available**: 26 pages, 7 figures and 4 tables. This material is
497 available free of charge via the Internet at http://pubs.acs.org.

498

499

500

501 **References**

502 1. Liu, J. Y.; Hsiao, T. C.; Lee, K. Y.; Chuang, H. C.; Cheng, T. J.; Chuang, K. J. Association
503 of ultrafine particles with cardiopulmonary health among adult subjects in the urban areas
504 of northern Taiwan. *Sci. Total Environ.* **2018**, *627*: 211-215.
505 2. Miller, M. R.; Raftis, J. B.; Langrish, J. P.; McLean, S. G.; Samutrtai, P.; Connell, S. P.;
506 Wilson, S.; Vesey, A. T.; Fokkens, P. H. B.; Boere, A. J. F.; Krystek, P.; Cambell, C. J.;
507 Hadoke, W. F.; Donaldson, K.; Cassee, F. R.; Newby, D. E.; Duffin, R.; Mills, N. L.
508 Inhaled nanoparticles accumulate at sites of vascular disease. *ACS nano.* **2017**, *11*(5):
509 4542-4552.
510 3. Stone, V.; Miller, M. R.; Clift, M. J. D.; Elder, A.; Mills, N. L.; Møller, P.; Schins, R. P. F.;
511 Vogel, U.; Kreyling, W. G.; Jensen, K. A.; Kuhlbusch, T. A. J.; Schwarze, P. E.; Hoet, P.;
512 Pietroiusti, A.; Vizcaya-Ruiz, A. D.; Baeza-Squiban, A.; Teixeira, J. P.; Tran, C. L.;
513 Cassee, F. R. Nanomaterials versus ambient ultrafine particles: an opportunity to

514 exchange toxicology knowledge. *Environ. Health Perspect.* **2017**, *125*(10): 106002. DOI:
515 10.1289/EHP424
516 4. Oberdörster, G.; Sharp, Z.; Atudorei, V.; Elder, A.; Gelein, R.; Kreyling, W.; Cox, C.
517 Translocation of inhaled ultrafine particles to the brain. *Inhal. Toxicol.* **2004**, *16*(6-7):
518 437-445.
519 5. Maher, B. A.; Ahmed, I. A. M.; Karloukovski, V.; MacLaren, D. A.; Foulds, P. G.; Allsop,
520 D.; Mann, D. M. A.; Torres-Jardón, R.; Calderon-Garduenas, L. Magnetite pollution
521 nanoparticles in the human brain. *P Natl. Acad. Sci. USA.* **2016**, *113*(39): 10797-10801.
522 6. Bakand, S.; Hayes, A.; Dechsakulthorn, F. Nanoparticles: a review of particle toxicology
523 following inhalation exposure. *Inhal. Toxicol.* **2012**, *24*(2): 125-135.
524 7. Donaldson, K.; Stone, V.; Seaton, A.; MacNee, W. Ambient particle inhalation and the
525 cardiovascular system: potential mechanisms. *Environ. Health Perspect.* **2001**, *109*(4):
526 523-527.
527 8. Karlsson, H. L.; Gustafsson, J.; Cronholm, P.; Möller, L. Size-dependent toxicity of metal
528 oxide particles—a comparison between nano-and micrometer size. *Toxicol. Lett.* **2009**,
529 *188*(2): 112-118.
530 9. Rückerl, R.; Schneider, A.; Breitner, S.; Cyrys, J.; Peters, A. Health effects of particulate
531 air pollution: a review of epidemiological evidence. *Inhal. Toxicol.* **2011**, *23*(10): 555-
532 592.
533 10. Hama, S. M. L.; Cordell R L.; Monks, P. S. Quantifying primary and secondary source
534 contributions to ultrafine particles in the UK urban background. *Atmos. Environ*. **2017**,

166: 62-78.

11. Shi, J. P.; Harrison, R. M.; Brear, F. Particle size distribution from a modern heavy duty diesel engine. *Sci. Total Environ.* **1999**, *235*(1-3): 305-317.

12. Maher, B. A.; Ahmed, I. A. M.; Davison, B.; Karloukovski, V.; Clarke, R. Impact of roadside tree lines on indoor concentrations of traffic derived particulate matter. *Environ. Sci. Technol.* **2013**, *47*: 13737-13744.

13. Liati, A.; Schreiber, D.; Dimopoulos Eggenschwiler, P.; Arroyo Rojas Dasilva, Y. Metal particle emissions in the exhaust stream of diesel engines: an electron microscope study. *Environ. Sci. Technol.* **2013**, *47*(24): 14495-14501.

14. Zhu, Y. F.; Hinds, W. C.; Kin, S.; Sioutas, C. Concentration and size distribution of ultrafine particles near a major highway. *Air Waste Manage. Assoc.* **2002**, *52*: 1032-1042.

15. Liati, A.; Pandurangi, S. S.; Boulouchos, K.; Schreiber, D.; Arroyo Rojas Dasilva, Y. Metal nanoparticles in diesel exhaust derived by in-cylinder melting of detached engine fragments. *Atmos. Environ*. **2015**, *101*: 34-40.

16. Kukutschová, J.; Moravec, P.; Tomášek, V.; Matějka, V.; Smolík, J.; Schwarz, J.; Seiderová, J.; Šafářová, K.; Filip, P. On airborne nano/micro-sized wear particles released from low-metallic automotive brakes. *Environ. Pollut.* **2011**, *159*(4): 998-1006.

17. Mathissen, M.; Scheer, V.; Vogt, R.; Benter, T. Investigation on the potential generation of ultrafine partilces from the tire-road interface. *Atmos. Environ*. **2011**, *45*(34): 6172-6179.

18. Yang, Y.; Vance, M.; Tou, F. Y.; Tiwari, A.; Liu, M.; Hochella Jr, M. F. Nanoparticles in road dust from impervious urban surfaces: distribution, identification, and environmental

implications. *Environ. Sci. Nano.* **2016**, *3*(3): 534-544.

19. Verma, V.; Shafer, M. M.; Schauer, J. J.; Sioutas, C. Contribution of transition metals in the reactive oxygen species activity of PM emissions from retrofitted heavy-duty vehicles. *Atmos. Environ*. **2010**, *44*, 5165-5173.

20. Sanderson, P.; Su, S. S.; Chang, I. T. H.; Delgado Saborit, J. M.; Kepaptsoglou, D. M.; Weber, R. J. M.; Harrison, R. M. Characterisation of iron-rich atmospheric submicrometre particles in the roadside environment. *Atmos. Environ*. **2016**, *140*: 167-175.

21. Harrison, R. M.; Shi, J. P.; Xi, S. H.; Khan, A.; Mark, D.; Kinnersley, R.; Yin, J. X. Measurement of number, mass and size distribution of particles in the atmosphere. *Philos. T. Roy. Soc. A.* **2000**, *358*(1775): 2567-2580.

22. Heal, M. R.; Kumar, P.; Harrison, R. M. Particles, air quality, policy and health. *Chem. Soc. Rev.* **2012**, *41*(19): 6606-6630.

23. Robert, M. A.; Kleeman, M. J.; Jakober, C. A. Size and composition distributions of particulate matter emissions: Part 2—Heavy-duty diesel vehicles. *J. Air Waste Manage. Assoc.* **2007**, *57*(12): 1429-1438.

24. Robert, M. A.; VanBergen, S.; Kleeman, M. J.; Jakober, C. A. Size and composition distributions of particulate matter emissions: Part 1—Light-duty gasoline vehicles. *J. Air Waste Manage. Assoc.* **2007**, *57*(12): 1414-1428.

25. Jayaratne, E. R.; He, C.; Ristovski, Z. D.; Morawska, L.; Johnson, G. R. A comparative investigation of ultrafine particle number and mass emissions from a fleet of road-road diesel and CNG buses. *Environ. Sci. Technol.* **2008**, *42*: 6736-6742.

26. Herner, J. D.; Hu, S. H.; Robertson, W. H.; Huai, T.; Chang, M. C. O.; Rieger, P.; Ayala, A. Effect of advanced aftertreatment for PM and NOx reduction on heavy-duty diesel engine ultrafine particle emissions. *Environ. Sci. Technol.* **2011**, *45*(6): 2413-2419.

27. Su, D. S.; Serafino, A.; Müller, J. O.; Jentoft, R. E.; Schlögl, R.; Fiorito, S. Cytotoxicity and inflammatory potential of soot particles of low-emission diesel engines. *Environ. Sci. Technol.* **2008**, *42*(5): 1761-1765.

28. Air Quality Expert Group. Impacts of vegetation on urban air pollution. **2018**, 1-40. https://uk-https://uk-air.defra.gov.uk/assets/documents/reports/cat09/1807251306180509_Effects_of_vegetation_on_urban_air_pollution_v12_final.pdf

29. Janhäll, S. Review on urban vegetation and particle air pollution–Deposition and dispersion. *Atmos. Environ*. **2015**, *105*: 130-137.

30. Jeanjean, A. P. R.; Monks, P. S.; Leigh, R. J. Modelling the effectiveness of urban trees and grass on $PM_{2.5}$ reduction via dispersion and deposition at a city scale. *Atmos. Environ*. **2016**, *147*: 1-10.

31. Jeanjean, A. P. R.; Buccolieri, R.; Eddy, J.; Monks, P. S.; Leigh, R. J. Air quality affected by trees in real street canyons: The case of Marylebone neighbourhood in central London. *Urban For. Urban Green.* **2017**, *22*: 41-53.

32. Nowak, D. J.; Hirabayashi, S.; Bodine, A.; Hoehn, R. Modeled $PM_{2.5}$ removal by trees in ten US cities and associated health effects. *Environ. Pollut.* **2013**, *178*: 395-402.

33. Vos, P. E. J.; Maiheu, B.; Vankerkom, J.; Janssen, S. Improving local air quality in cities: to tree or not to tree? *Environ. Pollut.* **2013**, *183*: 113-122.

598 34. Abhijith, K. V.; Kumar, P.; Gallagher, J.; MaNabola, A.; Baldauf, R.; Pilla, F.; Broderick,
599 B.; Di Sabatino, S.; Pulvirenti, B. Air pollution abatement performances of green
600 infrastructure in open road and built-up street canyon environments–A review. *Atmos.*
601 *Environ*. **2017**, *162*: 71-86.
602 35. Santiago, J. L.; Martilli, A.; Martin, F. On dry deposition modelling of atmospheric
603 pollutants on vegetation at the microscale: Application to the impact of street vegetation
604 on air quality. *Bound.-Layer Meteor.* **2017**, *162*(3): 451-474.
605 36. Burkhardt, J.; Peters, K.; Crossley, A. The presence of structural surface waxes on
606 coniferous needles affects the pattern of dry deposition of fine particles. *J. Exp. Bot.*
607 **1995**, *46*(7): 823-831.
608 37. Beckett, K. P.; Freer-Smith, P. H.; Taylor, G. Particulate pollution capture by urban trees:
609 effect of species and windspeed. *Glob. Change Biol.* **2000**, *6*(8): 995-1003.
610 38. Thönnessen, M. Elementdynamik in fassadenbegrünendemWilden Wein (*Parthenocissus*
611 *tricuspidata*). Nährelemente, Anorganische Schadstoffe, Platin-Gruppen-Elemente,
612 Filterleistung, Immissionshistorische Aspekte, Methodische Neu-
613 undWeiterentwicklungen. – Kölner Geographische Arbeiten, Heft 78, Geographisches
614 Institut, Universität Köln 2002; pp 103.
615 39. Mitchell, R.; Maher, B. A.; Kinnersley, R. Rates of particulate matter pollution deposition
616 onto leaf surfaces: temporal and inter-species magnetic analyses. *Environ. Pollut.* **2010**,
617 *158*: 1472-1478.
618 40. Weber, F.; Kowarik, I.; Säumel, I. Herbaceous plants as filters: Immobilization of

particulates along urban street corridors. *Environ. Pollut.* **2014**, *186*: 234-240.

41. *Airborne particulate matter in the United Kingdom*; Third report to the Department of the Environment; Quality of Urban Air Review Group (QUARG); HMSO, London, 1996; http://worldcat.org/isbn/0952077132.

42. Gallagher, M. W.; Beswick, K. M.; Duyzer, J.; Westrate, H.; Choularton, T. W.; Hummelshøj, P. Measurements of aerosol fluxes to Speulder forest using a micrometeorological technique. *Atmos. Environ*. **1997**, *31*(3): 359-373.

43. Freer-Smith, P. H.; Beckett, K. P.; Taylor, G. Deposition velocities to *Sorbus aria*, *Acer campestre*, *Populus deltoides* × *trichocarpa* 'Beaupré', *Pinus nigra* and × *Cupressocyparis leylandii* for coarse, fine and ultra-fine particles in the urban environment. *Environ. Pollut.* **2005**, *133*(1): 157-167.

44. Pugh, T. A. M.; Mackenzie, A. R.; Whyatt, J. D.; Hewitt, C. N. Effectiveness of green infrastructure for improvement of air quality in urban street canyons. *Environ. Sci. Technol.* **2012**, *46*(14): 7692-7699.

45. Nowak, D. J.; Crane, D. E.; Stevens, J. C. Air pollution removal by urban trees and shrubs in the United States. *Urban For. Urban Green.* **2006**, *4*(3): 115-123.

46. Litschke, T.; Kuttler, W. On the reduction of urban particle concentration by vegetation–a review. *Meteorol. Z.* **2008**, *17*(3): 229-240.

47. Jin, S. J.; Guo, J. K.; Wheeler, S.; Kan, L. Y.; Che, S. Q. Evaluation of impacts of trees on $PM_{2.5}$ dispersion in urban streets. *Atmos. Environ*. **2014**, *99*: 277-287.

48. Bonn, B.; von Schneidemesser, E.; Butler, T.; Churkina, G.; Ehlers, C.; Grote, R.; Klemp,

640 D.; Nothard, R.; Schäfer, K.; von Stülpnagel, A.; Kerschbaumer, A.; Yousefpour, R.;
641 Fountoukis, C.; Lawrence, M. G. Impact of vegetative emissions on urban ozone and
642 biogenic secondary organic aerosol: Box model study for Berlin, Germany. *J. Clean Prod.*
643 **2018**, *176*: 827-841.
644 49. Calfapietra, C.; Fares, S.; Manes, F.; Morani, A.; Sgrigna, G.; Loreto, F. Role of Biogenic
645 Volatile Organic Compounds (BVOC) emitted by urban trees on ozone concentration in
646 cities: A review. *Environ. Pollut.* **2013**, *183*: 71-80.
647 50. Hoffmann, T.; Odum, J. R.; Bowman, F.; Atmospheric, D. C. J. O. Formation of organic
648 aerosols from the oxidation of biogenic hydrocarbons. *J. Atmos. Chem.* **1997**, *26*, 189-222.
649 51. Matzka, J.; Maher, B. A. Magnetic biomonitoring of roadside tree leaves: identification of
650 spatial and temporal variations in vehicle-derived particulates. *Atmos. Environ*. **1999**, *31*:
651 4565-4569.
652 52. Fowler, D.; Skiba, U.; Nemitz, E.; Choubedar, F.; Branford, D.; Donovan, R.; Rowland, P.
653 Measuring aerosol and heavy metal deposition on urban woodland and grass using
654 inventories of ^{210}Pb and metal concentrations in soil. *Water Air Soil Pollut. Focus.* **2004**,
655 *4*: 483-499.
656 53. Baldauf, R.; Thoma, E.; Khlystov, A.; Isakov, V.; Bowker, G.; Long, T.; Snow, R. Impacts
657 of noise barriers on near-road air quality. *Atmos. Environ*. **2008**, *42*(32): 7502-7507.
658 54. Al-Dabbous, A. N.; Kumar, P. The influence of roadside vegetation barriers on airborne
659 nanoparticles and pedestrians exposure under varying wind conditions. *Atmos. Environ*.
660 **2014**, *90*(90): 113-124.

661 55. Lin, M. Y.; Hagler, G.; Baldauf, R.; Isakov, V.; Lin, H. Y.; Khlystov, A. The effects of
662 vegetation barriers on near-road ultrafine particle number and carbon monoxide
663 concentrations. *Sci. Total Environ.* **2016**, *553*: 372-379.
664 56. Lin, M. Y.; Khlystov, A. Investigation of ultrafine particle deposition to vegetation
665 branches in a wind tunnel. *Aerosol Sci. Technol.* **2011**, *46*: 465-472.
666 57. Hwang, H. J.; Yook, S. J.; Ahn, K. H. Experimental investigation of submicron and
667 ultrafine soot particle removal by tree leaves. *Atmos. Environ*. **2011**, *45*: 6987-6994.
668 58. Davison, B.; Whyatt, D.; Boardman, C. Aerosol evolution from a busy road in North-west
669 England. *Meteorogische Zeitschrift*. **2008**, *18*(1): 55-60.
670 59. Maher, B. A. Magnetic properties of some synthetic sub-micro magnetites. *Geophys. J.*
671 *Int.* **1988**, *94*: 83-96.
672 60. Maher, B. A.; Karloukovski, V. V.; Mutch, T. J. High-field remanence properties of
673 synthetic and natural submicrometre haematites and goethites: significance for
674 environmental contexts. *Earth Planet. Sci. Lett.* **2004**, *226*(3-4): 491-505.
675 61. Lehndorff, E.; Urbat, M.; Schwark, L. Accumulation histories of magnetic particles on
676 pine needles as function of air quality. *Atmos. Environ*. **2006**, *40*(36): 7082-7096.
677 62. Wang, H. X.; Shi, H.; Li, Y. Y.; Zhang, J. Seasonal variations in leaf capturing of
678 particulate matter, surface wettability and micromorphology in urban tree species. *Front.*
679 *Env. Sci. Eng.* **2013**, *7*(4): 579-588.
680 63. Liu, J. Q.; Cao, Z. G.; Zou, S. Y.; Liu, H. H.; Hai, X.; Wang, S. H.; Duan, J.; Xi, B. Y.;
681 Yan, G. X.; Zhang, S. W.; Jia, Z. K. An investigation of the leaf retention capacity,

efficiency and mechanism for atmospheric particulate matter of five greening tree species in Beijing, China. *Sci. Total Environ.* **2018**, *616-617*: 417-426.

64. Weerakkody, U.; Dover, J. W.; Mitchell, P.; Reiling, K. Evaluating the impact of individual leaf traits on atmospheric particulate matter accumulation using natural and synthetic leaves. *Urban For. Urban Green.* **2018**, *30*: 98-107.

65. Hicks, B. B.; Saylor, R. D.; Baker, B. D. Dry deposition of particles to canopies—A look back and the road forward. *J. Geophys. Res.-Atmos.* **2016**, *121*(24): 14691-14707.

66. Moran, J. L.; Posner, J. D. Phoretic self-propulsion. *Annu. Rev. Fluid Mech.* **2017**, *49*: 511-540.

67. *The mortality effects of long-term exposure to particulate air pollution in the United Kingdom*; Committee on the Medical Effects of Air Pollutants, Department of Health, London, UK, 2010; http://comeap.org.uk/documents/reports/128-the-mortality-effects-of-long-term-exposure-toparticulate-air-pollution-in-the-uk.html.

697 TOC

698

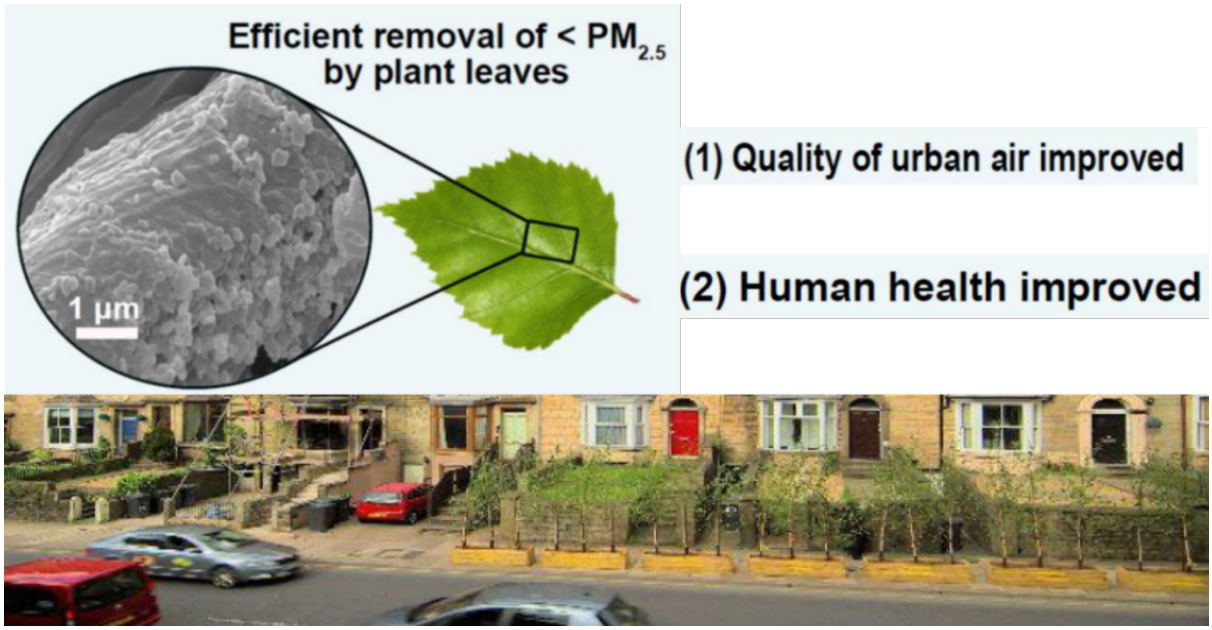

699

Supporting Information

Efficient removal of ultrafine particles from diesel exhaust by selected tree species: implications for roadside planting for improving the quality of urban air

Huixia Wang[1, 2], Barbara A Maher[2], Imad AM Ahmed[3] & Brian Davison[2]

[1] School of Environmental and Municipal Engineering, Xi'an University of Architecture & Technology, Xi'an, 710055, China

[2] Centre for Environmental Magnetism & Palaeomagnetism, Lancaster Environment Centre, University of Lancaster, Lancaster, LA1 4YQ, United Kingdom

[3] Department of Earth Sciences, University of Oxford, Oxford, OX1 3AN, United Kingdom

*Corresponding author. E-mail: b.maher@lancaster.ac.uk; Tel: +44 (0) 1524 510268; Fax: +44 (0) 1524 593985

This document contains 26 pages, 7 figures and 4 tables.

Figures:

Figure S1: Ratio of vegetation deposition flux to traffic emission flux depending on surface area of vegetation velocity (V_d) in a street canyon of 100 m length with annual PM_{10} concentration of 37 µg m^{-3}, average emission factor 100 µg $vehicle^{-1}$ m^{-1} for PM_{10}, traffic intensity of ~ 40000 vehicles d^{-1} (Adapted with permission from reference 1. Copyright 2008 Schweizerbart science publishers. Available at https://www.schweizerbart.de/journals/metz).

Figure S2: Schematic diagram showing the configuration of the wind tunnel experiments

Figure S3: Upwind particle number concentration and size distribution in the absence of any vegetation, and with vegetation.

Figure S4: $PM_{2.5}$ concentrations upwind and downwind of juniper.

Figure S5: Changes in magnetic particle loadings over successive diesel exposure intervals, as measured by ARM, IRM_{100}, IRM_{300} and SIRM.

Figure S6: The grain size of the magnetic particles deposited on the leaves of each species, pre-exposure (0 mins) and at successive time intervals of exposure, estimated from the χ_{ARM}/SIRM values (the grain size of the magnetic particles was calculated according to reference 2).

Figure S7: Aggregates and chains of particles deposited on the surface of a post-exposure birch leaf.

Tables:

Table S1: Summary of the vegetation attributes in the wind tunnel studies (*indicating adaptation with permission from reference 3. Copyright 2010 Elsevier.)

Table S2: The geomean diameter of the UFPs without vegetation, and downwind of each vegetation species

Table S3: Magnetic time series of leaf samples; parameter units (i.e. all values normalised by leaf surface area, m^2): χ_{ARM} ($\times 10^{-8}$A), SIRM ($\times 10^{-6}$A), χ_{ARM}/IRM_{100mT} ($\times 10^{-5}A^{-1}$), χ_{ARM}/IRM_{300mT} ($\times 10^{-5}A^{-1}$), χ_{ARM}/SIRM ($\times 10^{-5}A^{-1}$), $\%IRM_{100mT}$, $\%IRM_{300mT}$ and %HIRM for all leaf samples

Table S4: Leaf leachate metal enrichment ratios measured after exposure to diesel exhaust (i.e. metal concentration post-exposure/metal concentration pre-exposure).

Supporting Methods:

S1-1: *Plant Species*

Ten plant species including silver birch, yew, nettle, beech, cherry, elder, maple, hawthorn, ash and juniper were selected for their different leaf surface characteristics and particle deposition velocities. These species are also widespread in temperate regions, have different leaf retention behaviours (i.e., deciduous vs evergreen species) and different leaf morphologies (i.e., broad leaves vs needles) and micro-topographies, which are expected to have an influence on UFP deposition and accumulation.

S1-2: *Determination of Leaf Area Index*

At the end of the experiment, ~ 5% of the total leaves from each vegetation block was weighed (Oertling KC22 microbalance) then scanned, and leaf area measured through counting image pixels. Total foliage area was determined by the mass proportion of the scanned leaf weight to total weight and leaf area; the total leaf area was divided by the crown area to determine the leaf area index (LAI).

S1-3: *Magnetic Measurements*

Leaf samples of each species were collected before exposure to the diesel exhaust (here labelled as 0 minute) and then after successive exposure intervals (i.e. after 2, 5, 10, 20, 30, and 35 minutes), using gloves to avoid any contamination. The leaves

were stored (upper surface to upper surface) in ziplock bags, at 4 ℃, prior to scanning (5-6 leaves per individual species sample for one replicate), and then were packed into 10 cm^3 plastic pots for magnetic measurements. The magnetic measurements were made at the Centre for Environmental Magnetism and Palaeomagnetism, Lancaster University.

Anhysteretic remanent magnetization (ARM) is sensitive to the presence of ferrimagnetic particles with a mean particle size of ~25 nm (Maher, 1988). The saturation isothermal remanent magnetization (SIRM) indicates the total concentration of magnetic particles on the pre- and post-exposure leaves[2].

ARM was induced using a Molspin A. F. demagnetiser, with ARM attachment, generating a dc biasing field (0.08 mT) in the presence of an alternating field (100 milliTesla (mT) peak field). The ARM was measured using a spinner magnetometer (JR-6A, AGICO, Advanced Geoscience Instruments Co., Brno, Czech Republic). The susceptibility of ARM (χ_{ARM}) was calculated by normalizing the ARM by the dc biasing field.

Room temperature remanent magnetization (IRM) was incrementally acquired (in dc fields of 100 and 300 mT) using a Molspin pulse magnetizer. SIRM was acquired in the dc field of 1 T. IRM and SIRM also measured using JR-6A.

Calibration of the magnetometer was performed, on a regular basis, using a cross-calibrated rock sample (56.05×10^{-8} Am^2). All magnetic measurements were normalised for the leaf surface area (in m^2).

S1-4: ***Metals Analysis***

The leaf-deposited PM was evaluated by an acid wash procedure and analysis of metal(loid) concentrations using inductively coupled plasma-mass spectrometry (ICP-MS). Two leaves from each species, pre- and post-exposure, respectively, were washed thoroughly using purified 2% HNO_3 into an acid-cleaned centrifuge tube. The resultant leachate was then analysed for Mn, Fe, Co, Ni, Cu, Zn, Ti, V, Cr, As, Zr, Mo, Se, Cd, Sn, Sb, Pt and Pb using a Perkin Elmer quadrupole NexION 350D ICP-MS instrument. The elements of Se, Cd, Sn, Sb, Pt and Pb were measured under non-pressurised conditions (standard mode) whereas the remaining elements were measured in a collision cell with kinetic energy discrimination (collision mode) using helium gas. Metal compositions in the stock acid wash solution were well below 25 ng L^{-1}, except for Ti (< 65 ng L^{-1}) and Zn (< 201 ng L^{-1}), most likely a contribution from tubing used during the ICP-MS analysis.

Supplemental Figures and Tables:

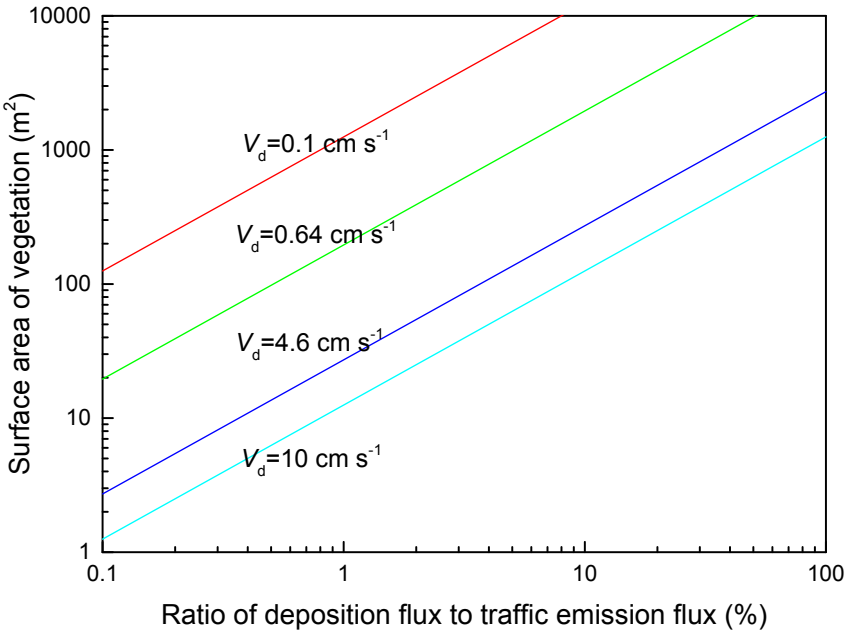

Fig. S1 Ratio of vegetation deposition flux to traffic emission flux depending on surface area of vegetation velocity (V_d) in a street canyon of 100 m length with annual PM_{10} concentration of 37 µg m^{-3}, average emission factor 100 µg $vehicle^{-1}$ m^{-1} for PM_{10}, traffic intensity of ~ 40000 vehicles d^{-1} (Adapted with permission from reference 1. Copyright 2008 Schweizerbart science publishers. Available at https://www.schweizerbart.de/journals/metz).

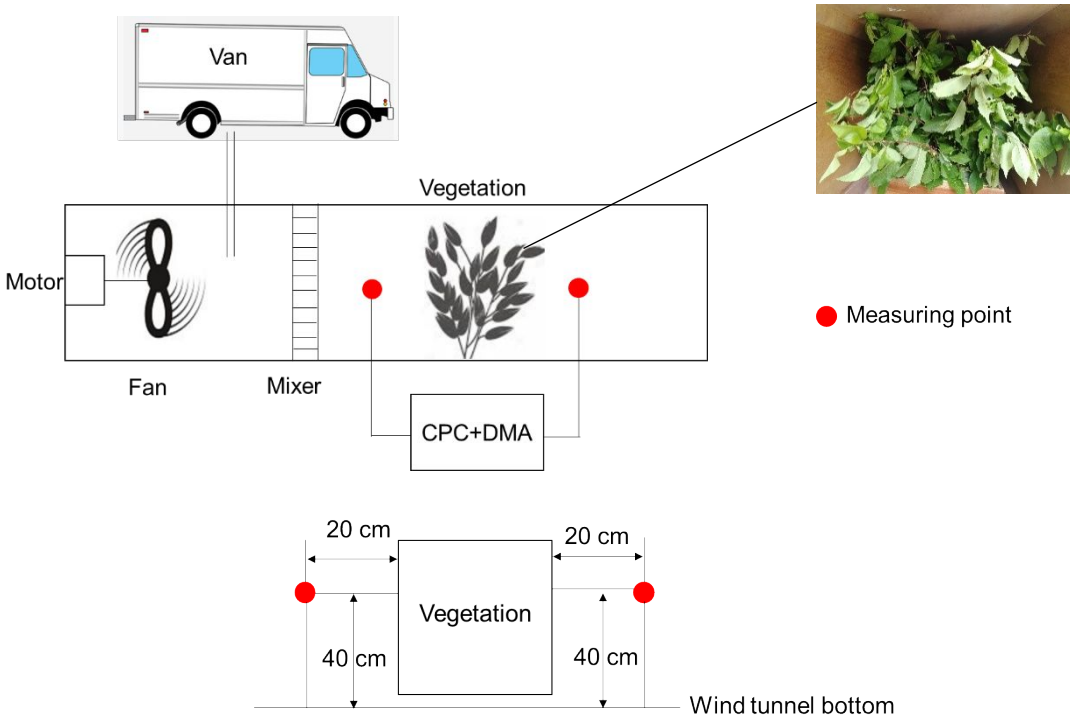

Fig. S2 Schematic diagram showing the configuration of the wind tunnel experiments

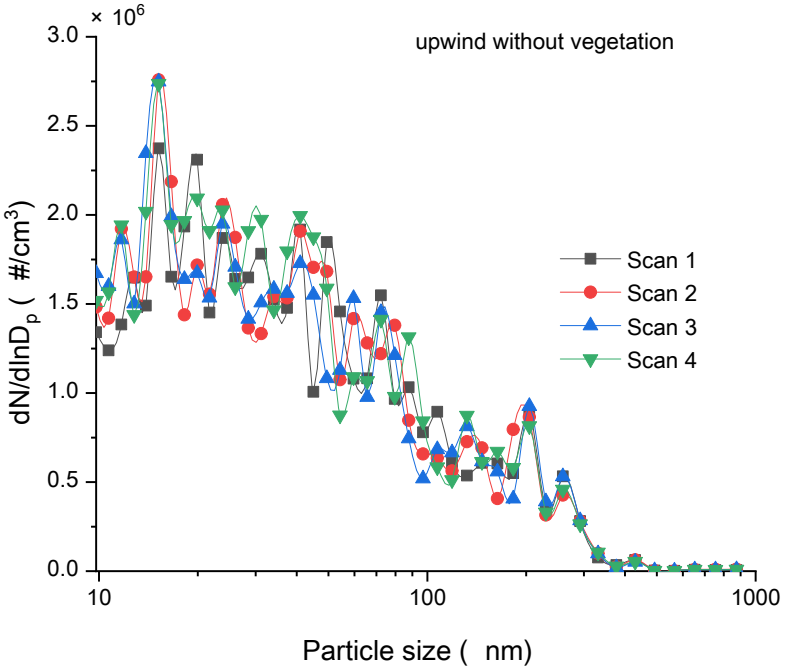
× 10^6
upwind without vegetation
dN/dlnD_p (#/cm^3)
Particle size (nm)
Scan 1
Scan 2
Scan 3
Scan 4

129

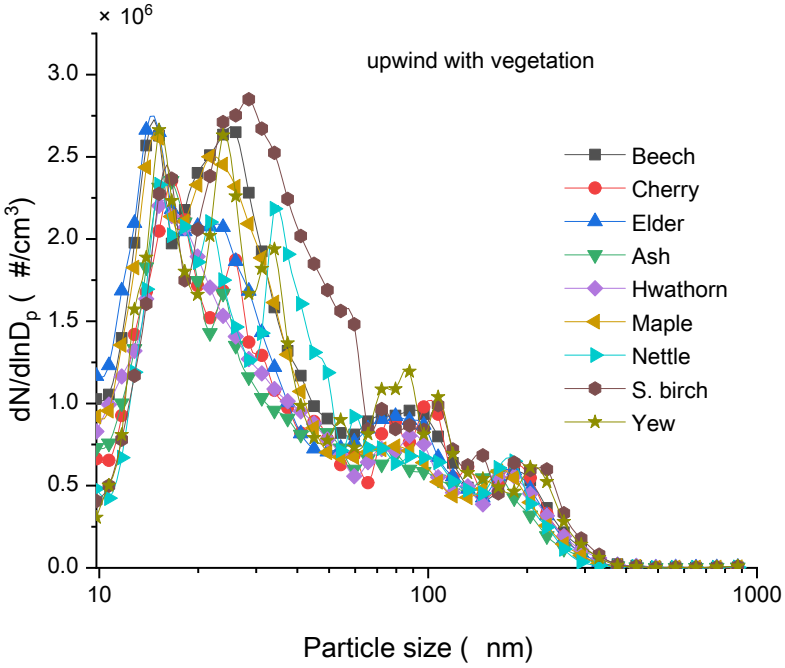
× 10^6
upwind with vegetation
dN/dlnD_p (#/cm^3)
Particle size (nm)
Beech
Cherry
Elder
Ash
Hwathorn
Maple
Nettle
S. birch
Yew

130

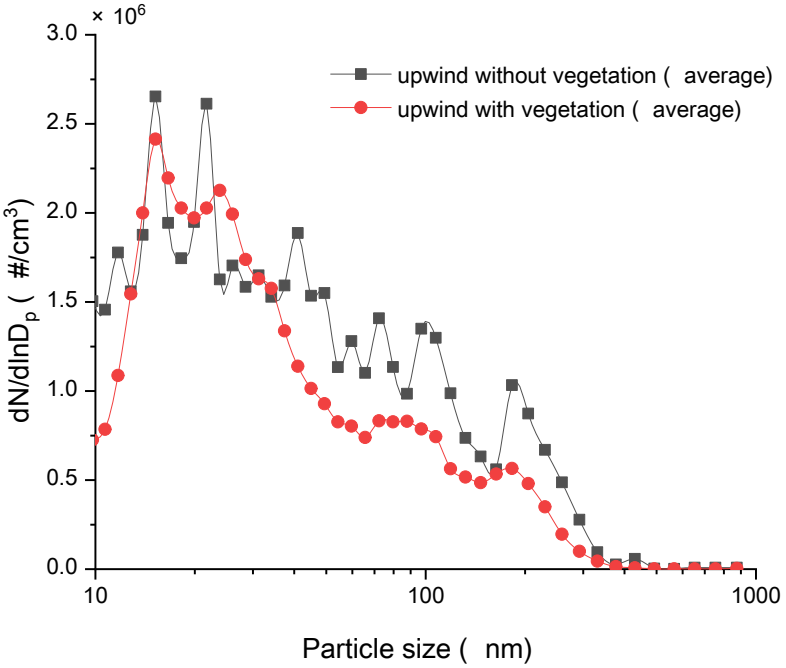

131

132 Fig. S3 Upwind particle number concentration and size distribution in the absence of

133 any vegetation and with vegetation.

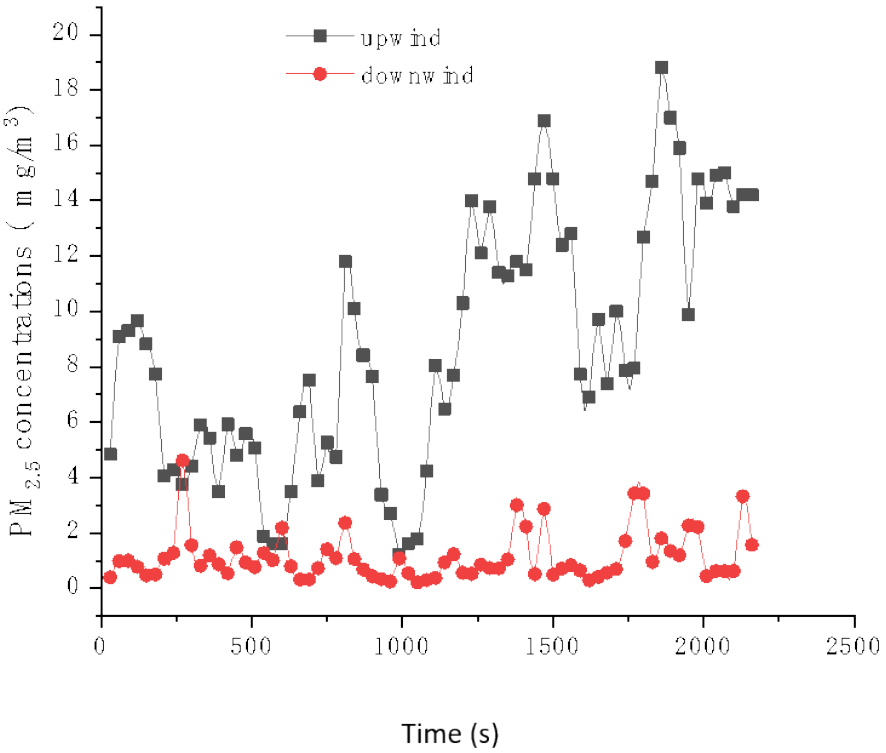

Fig. S4 $PM_{2.5}$ concentrations upwind and downwind of juniper.

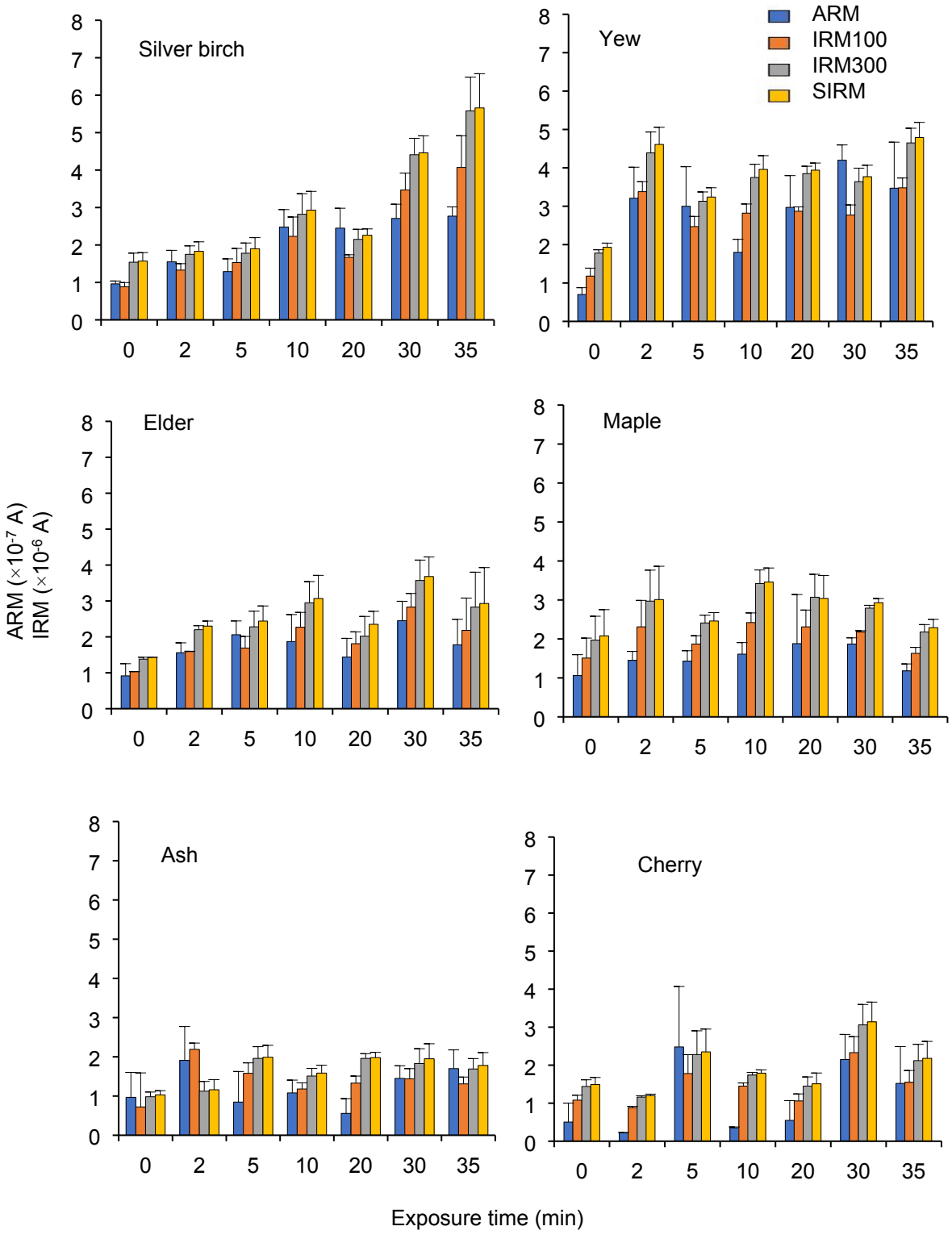
Silver birch
Yew
Elder
Maple
Ash
Cherry
ARM
IRM100
IRM300
SIRM
ARM (×10-7 A)
IRM (×10-6 A)
Exposure time (min)
0
2
5
10
20
30
35

141

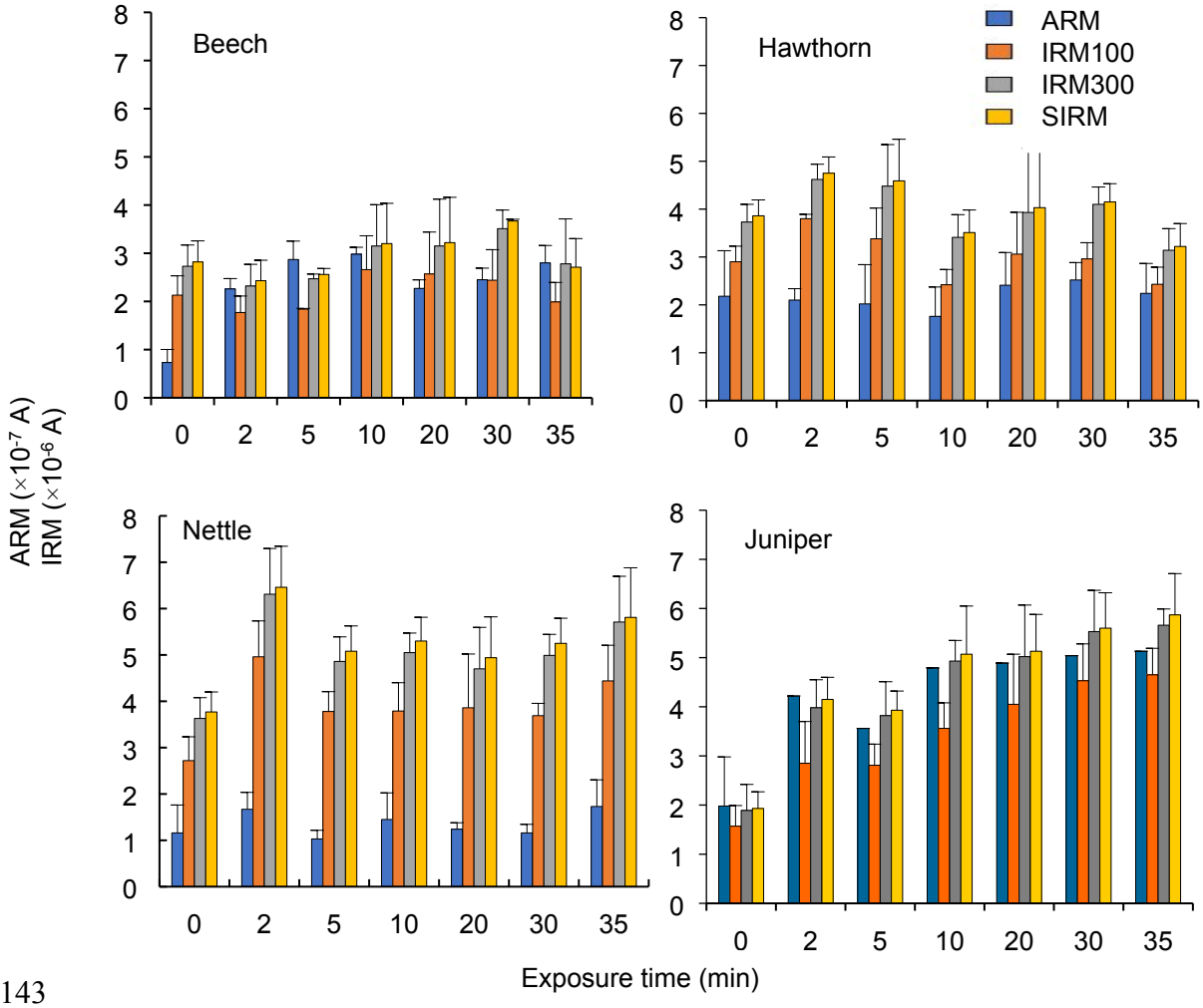

143

144 Fig. S5 Changes in magnetic particle loadings over successive diesel exposure

145 intervals, as measured by ARM, IRM_{100}, IRM_{300} and SIRM.

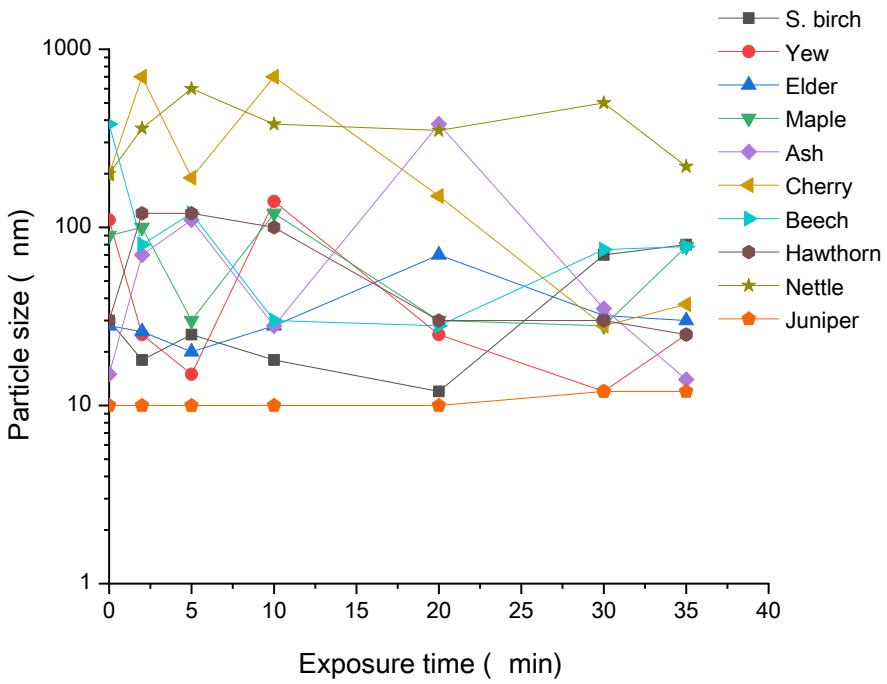

Fig. S6 The grain size of the magnetic particles deposited on the leaves of each species, pre-exposure (0 mins) and at successive time intervals of exposure, estimated from the χ_{ARM}/SIRM values (the grain size of the magnetic particles was calculated according to reference 2).

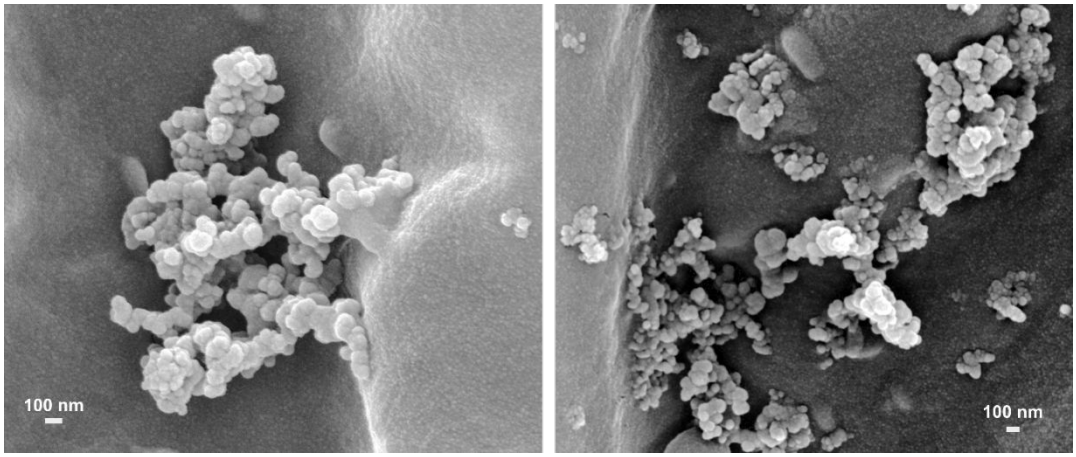

Figure S7. Aggregates and chains of particles deposited on the surface of a post-exposure birch leaf.

159 Table S1 Summary of the vegetation attributes in the wind tunnel studies (*indicating adaptation with permission from reference 3. Copyright

160 2010 Elsevier.)

Species	LAI	Deposition velocity ($cm\ s^{-1}$) [±1 S.E.]*	Leaf arrangement*	Shape*	Margin*	Surface*	
						Upper	Lower
Silver birch	8.53	4.6	Simple alternate	Deltoid	Doubly-serrate	Ridged	Hairy ridged
Yew	8.57						
Nettle	8.46						
Beech	8.43	3.0 [1.52]	Simple	Obtuse	Entire or ciliate	Ridged hairy	Hairy
Cherry	8.60						
Elder	7.30	0.8 [0.20]	Compound pinnate	Obtuse or falcate	Serrate	Smooth	Hairy
Maple	8.98	1.9 [0.46]	Simple opposite	Palmate	Entire	Smooth +'honeydew'	Ridged
Hawthorn	7.15						
Ash	8.80	1.5 [1.02]	Compound opposite	Obtuse	Serrate	Ridged	Hairy (young)
Juniper	8.25						

Table S2 The geomean diameter of the UFPs without vegetation and downwind of each vegetation species

Plant species	Geomean diameter (nm)	
	No vegetation	Downwind of vegetation
Silver birch	20.8	27.2
Yew	19.3	29.6
Nettle	21.5	22.3
Beech	19.0	19.9
Cherry	20.2	20.2
Elder	17.8	17.4
Maple	18.5	23.8
Hawthorn	18.8	18.0
Ash	18.8	19.2

Table S3 Magnetic time series of leaf samples; parameter units (i.e. all values normalised by leaf surface area, m^2): χ_{ARM} ($\times10^{-8}$A), SIRM ($\times10^{-6}$A), χ_{ARM}/IRM_{100mT} ($\times10^{-5}A^{-1}$), χ_{ARM}/IRM_{300mT} ($\times10^{-5}A^{-1}$), χ_{ARM}/SIRM ($\times10^{-5}A^{-1}$), $\%IRM_{100mT}$, $\%IRM_{300mT}$ and %HIRM for all leaf samples

Plant species	Time (minutes)	χ_{ARM}	SIRM	χ_{ARM}/IRM_{100mT}	χ_{ARM}/IRM_{300mT}	χ_{ARM}/SIRM	%HIRM	$\%IRM_{100mT}$	$\%IRM_{300mT}$
	0	12.1±0.1	1.6±0.2	139.2±27.4	79.5±9.6	77.7±8.8	2.2±1.5	57.6±15.0	97.8±1.5
	2	19.5±3.9	1.8±0.3	150.9±44.9	114.6±34.0	109.8±33.5	4.3±1.1	72.8±3.0	95.7±1.1
	5	16.3±4.3	1.9±0.3	115.8±57.2	94.8±36.9	88.5±34.2	6.5±1.5	79.4±9.3	93.5±1.5
S. birch	10	31.2±5.8	2.9±0.5	141.0±11.8	110.9±11.5	106.7±13.2	3.9±3.3	75.7±7.0	96.1±3.3
	20	30.8±6.7	2.3±0.2	185.4±47.6	147.5±52.0	138.2±40.9	5.1±5.0	74.1±3.0	94.9±5.0
	30	34.1±4.8	4.5±0.5	99.8±21.7	77.4±9.1	76.5±9.5	1.1±0.6	77.8±7.8	98.9±0.6
	35	34.8±3.1	5.7±0.9	87.3±14.6	63.2±8.7	62.3±8.4	1.4±0.4	71.7±3.2	98.6±0.4

	0	8.8±2.2	1.9±0.1	73.7±5.7	49.2±11.0	45.6±10.3	7.5±1.2	61.3±9.1	92.5±1.2
	2	40.4±10.1	4.6±0.4	121.3±37.6	94.6±33.2	89.4±29.1	4.9±4.2	73.4±1.6	95.1±4.2
	5	37.7±13.0	3.2±0.2	150.6±41.7	118.6±32.9	114.9±32.8	3.3±1.0	76.1±3.0	96.7±1.0
Yew	10	22.6±4.3	4.0±0.4	79.9±10.7	60.1±7.9	56.7±6.3	5.4±2.8	71.2±2.0	94.6±2.8
	20	37.3±10.4	3.9±0.2	130.8±40.4	96.8±26.9	94.6±25.9	2.2±0.6	73.1±4.4	97.8±0.6
	30	52.8±5.0	3.8±0.3	191.6±21.5	145.8±15.0	140.6±15.5	3.5±2.7	73.4±1.4	96.5±2.7
	35	43.6±15.1	4.8±0.4	124.9±39.0	94.6±33.6	91.8±32.4	3.0±0.2	72.8±3.2	97.0±0.2
	0	14.5±7.6	3.8±0.4	54.1±25.8	39.6±17.8	38.1±17.2	3.9±1.0	71.9±7.1	96.1±1.0
	2	20.9±4.6	6.5±0.9	42.9±11.9	33.9±10.0	32.9±9.1	2.4±2.1	76.7±2.0	97.6±2.1
Nettle	5	12.9±2.4	5.1±0.5	34.8±9.3	27.1±7.5	25.8±6.6	4.5±2.5	74.2±0.9	95.5±2.5
	10	18.2±7.2	5.3±0.5	48.5±17.6	35.8±13.1	34.5±13.0	4.1±1.9	71.3±5.0	95.9±1.9
	20	15.5±1.7	4.9±0.9	42.5±11.8	33.6±5.3	31.9±4.6	4.9±1.7	77.0±11.0	95.1±1.7

	30	14.5±2.3	5.3±0.5	39.8±8.8	29.2±4.2	27.7±3.9	4.9±1.2	70.6±7.7	95.1±1.2
	35	21.8±7.2	5.8±1.1	48.3±7.3	37.5±5.7	36.9±5.2	1.6±1.2	76.5±1.2	98.4±1.2
	0	9.2±3.4	2.8±0.4	46.2±23.8	35.6±17.2	34.4±16.6	3.2±1.7	75.3±3.0	96.8±1.7
	2	14.9±3.5	2.4±0.4	86.1±23.3	65.7±17.1	62.4±15.5	4.9±2.1	72.8±2.0	95.1±2.1
	5	12.2±3.5	2.6±0.1	66.1±18.6	49.1±12.8	47.5±12.2	3.3±0.9	72.1±2.9	96.7±0.9
Beech	10	32.4±13.2	3.9±0.8	104.4±25.2	83.2±21.8	81.7±22.0	2.0±1.1	77.8±2.5	98.0±1.1
	20	28.5±22.4	3.2±0.9	100.5±49.9	82.3±43.1	80.5±43.6	2.7±1.8	78.9±4.2	97.3±1.8
	30	12.8±6.7	2.0±0.4	86.4±43.1	66.2±34.0	64.3±33.1	2.9±0.2	73.7±2.1	97.1±0.2
	35	19.0±9.9	2.7±0.6	94.4±38.4	71.2±28.6	69.3±27.8	2.7±0.2	73.5±1.3	97.3±0.2
	0	6.3±6.3	1.5±0.2	55.9±50.2	41.7±37.2	40.2±35.6	3.3±0.7	72.7±1.4	96.7±0.7
Cherry	2	2.8±0.1	1.2±0.1	32.2±1.2	24.4±0.9	23.6±0.9	3.4±0.3	73.2±1.8	96.6±0.3
	5	31.1±19.9	2.4±0.6	84.7±16.0	46.6±10.9	41.0±9.5	3.1±1.8	75.3±4.9	96.9±1.8

	10	4.4±0.3	1.8±0.1	30.5±3.2	25.3±0.8	24.6±0.6	2.8±1.0	81.2±6.9	97.2±1.0
	20	6.9±6.5	1.5±0.3	62.0±52.9	45.0±37.5	42.9±35.1	4.0±2.3	70.5±2.5	96.0±2.3
	30	27.0±8.2	3.1±0.5	114.4±13.7	87.2±10.9	85.0±11.4	2.6±1.8	74.2±1.2	97.4±1.8
	35	19.1±12.2	2.2±0.4	116.4±59.4	84.9±43.2	82.3±41.6	2.7±1.2	71.0±1.1	97.3±1.2
	0	11.5±4.2	1.4±0.1	111.5±40.6	83.7±31.8	80.9±31.7	3.7±1.5	72.0±2.4	96.3±1.5
	2	19.6±3.5	2.3±0.1	123.8±22.7	89.0±11.5	85.1±10.2	4.3±1.4	69.5±6.2	95.7±1.4
	5	25.9±4.8	2.4±0.4	153.5±2.4	114.0±9.2	106.7±9.8	6.5±2.4	69.6±7.4	93.5±2.4
Elder	10	23.4±9.4	3.1±0.6	108.0±49.7	83.7±39.9	80.8±38.9	3.7±0.9	74.1±2.3	96.3±0.9
	20	18.0±6.5	2.4±0.4	97.9±23.3	88.8±19.7	75.0±16.4	4.8±2.8	77.0±8.0	85.2±12.8
	30	30.8±6.8	3.7±0.5	108.4±12.6	86.1±11.3	83.6±11.4	2.9±1.0	77.0±2.6	97.1±1.0
	35	22.4±8.9	2.9±0.1	112.2±62.0	84.9±47.3	82.2±46.8	3.5±1.4	73.2±6.2	96.5±1.4
Maple	0	13.3±6.7	2.1±0.7	90.7±41.1	68.9±31.0	65.9±30.1	4.8±1.4	72.6±1.4	95.2±1.4

	2	18.2±2.9	3.0±0.9	82.0±21.6	63.4±16.6	63.0±17.8	1.0±1.0	76.6±2.4	99.0±1.9
	5	18.0±3.4	2.5±0.2	96.3±13.2	74.4±10.6	73.0±9.9	1.7±0.8	75.9±2.1	98.3±0.8
	10	20.2±3.7	3.5±0.4	83.1±8.1	58.9±7.3	58.2±6.7	1.2±0.8	70.2±6.7	98.8±0.8
	20	23.7±15.8	3.0±0.6	96.9±60.8	73.6±45.0	72.9±44.4	1.1±1.0	76.2±2.5	99.1±0.9
	30	23.5±2.0	2.9±0.1	107.8±7.9	84.4±5.9	80.1±3.9	5.0±2.4	74.4±1.9	95.0±2.4
	35	14.8±2.3	2.3±0.2	90.8±9.6	67.8±6.3	64.6±6.3	4.7±1.0	71.2±0.6	95.3±1.0
	0	27.4±11.9	3.9±0.3	98.6±55.3	75.0±38.8	72.5±37.0	3.2±1.3	75.1±6.3	96.8±1.3
	2	26.4±3.0	4.8±0.3	69.3±6.3	57.0±2.7	55.4±2.4	2.8±0.6	80.2±4.2	97.2±0.6
	5	25.4±10.3	4.6±0.9	73.4±15.9	55.5±12.2	54.1±11.9	2.6±0.9	73.6±0.5	97.4±0.9
Hawthorn	10	22.1±7.7	3.5±0.5	91.9±34.0	65.3±24.3	63.4±23.5	2.9±0.5	69.0±0.2	97.1±0.5
	20	30.3±8.6	4.0±1.4	108.2±49.2	86.7±42.2	84.5±41.4	2.4±0.1	77.0±5.1	97.6±0.1
	30	31.7±4.6	4.2±0.4	107.1±10.5	77.4±9.9	76.5±9.7	1.2±0.4	71.4±2.8	98.8±0.4

	35	28.2±7.9	3.2±0.5	114.7±19.5	89.0±16.7	86.7±15.5	2.5±1.0	75.5±1.0	97.5±1.0
	0	12.1±8.0	1.0±0.1	177.2±121.7	126.7±85.2	120.3±80.4	4.9±2.1	70.1±5.7	95.1±2.1
	2	24.0±10.9	3.2±0.3	109.0±46.3	75.3±27.9	74.5±27.4	1.1±0.2	69.4±4.5	98.9±0.2
	5	10.6±9.8	2.0±0.3	63.4±56.5	50.2±42.4	49.6±42.3	1.5±1.3	79.1±4.6	98.5±1.3
Ash	10	13.6±4.1	1.6±0.2	115.5±35.6	89.5±24.6	85.0±19.9	4.5±3.6	74.6±5.0	95.5±3.6
	20	7.0±4.7	2.0±0.1	51.4±34.1	35.1±22.7	34.6±22.4	1.3±0.7	66.9±5.2	98.7±0.7
	30	30.8±4.1	3.4±0.4	126.2±3.4	93.2±3.1	91.9±3.5	1.5±0.5	72.8±1.6	98.5±0.5
	35	21.4±6.0	2.8±0.3	165.2±45.5	129.0±38.1	122.0±35.3	5.2±3.6	73.7±4.0	94.8±3.6
	0	24.9±6.9	1.9±0.3	158.5±23.9	131.6±21.2	128.9±19.7	2.1±0.5	81.3±4.3	97.9±1.3
	2	53.0±13.5	4.2±0.5	186.1±43.2	133.2±35.8	127.8±33.2	4.1±1.5	68.7±4.2	95.9±0.8
Juniper	5	44.7±9.6	3.9±0.4	159.2±19.7	117.1±17.6	113.8±15.9	2.8±0.5	71.5±3.6	97.2±2.0
	10	60.2±12.3	5.1±1.0	169.1±21.3	122.1±19.4	118.7±18.9	2.8±0.7	70.2±1.4	97.2±1.8

20	61.4±8.9	5.1±0.8	151.7±15.9	122.4±14.3	119.8±13.5	2.1±1.2	78.9±2.6	97.9±0.9
30	63.3±23.2	5.6±0.7	139.8±10.7	114.5±9.9	113.1±9.7	1.3±0.4	80.9±3.9	98.8±1.1
35	64.5±12.6	5.9±0.8	138.6±19.4	113.9±16.7	109.8±15.3	3.6±1.3	79.2±1.1	96.4±3.2

166

Table S4 Leaf leachate metal enrichment ratios measured after exposure to diesel exhaust (i.e. metal concentration post-exposure/metal concentration pre-exposure).

	Ash	Maple	Beech	Cherry	Yew	Hawthorn	S. birch
Mn	1.98	18.00	14.03	3.24	14.94	10.06	17.27
Fe	1.45	2.36	1.13	1.17	1.85	4.06	2.77
Co	4.98	3.30	10.00	1.51	2.31	2.23	11.88
Ni	4.18	4.46	1.11	1.46	8.15	1.53	5.91
Cu	1.79	2.70	1.36	1.55	18.30	2.56	2.98
Zn	2.27	2.80	1.52	1.99	7.32	1.25	2.63
Ti	2.68	3.66	2.87	1.76	2.03	2.41	4.00
V	28.60	43.97	14.71	5.25	70.87	27.12	17.26
Cr	15.17	12.03	6.44	6.98	26.18	19.93	14.62
As	2.00	2.07	1.84	1.74	3.47	7.39	10.21
Zr	1.95	1.56	6.48	8.20	4.46	4.82	8.47
Mo	1.87	1.82	4.57	1.50	4.47	2.29	1.22
Se	1.17	2.17	1.23	3.37	3.65	5.35	6.59
Cd	18.38	1.10	9.45	2.31	10.56	2.09	7.51
Pt	4.09	4.15	2.75	3.02	1.14	1.77	12.89
Pb	1.44	4.48	7.38	4.02	2.60	1.89	4.94

REFERENCES

1. Litschke, T.; Kuttler, W. On the reduction of urban particle concentration by vegetation–a review. *Meteorol. Z.* **2008**, *17*(3): 229-240.
2. Maher, B. A. Magnetic properties of some synthetic sub-micro magnetites. *Geophys. J. Int.* **1988**, *94*: 83-96.
3. Mitchell, R.; Maher, B. A.; Kinnersley, R. Rates of particulate matter pollution deposition onto leaf surfaces: temporal and inter-species magnetic analyses. *Environ. Pollut.* **2010**, *158*: 1472-1478.